fermentation

MDPI

Article

Defining the Fermentation Endpoint of *Lactiplantibacillus plantarum*-Fermented *Sparassis latifolia* Superfine Powder by an Integrated Multi-Analytical and Metabolomic Approach

Zhiao Wu [1,†], Zihao Kong [2,†], Bin Wang [1], Yuan Lin [1], Jianming Huang [1], Zhanxian Le [3], Liangyi Zhang [4], Xinyi Liu [1] and Di Zhang [2,*]

[1] Fujian Institute of Testing Technology, Fuzhou 350003, China; jszy01@fjitt.com (Z.W.)
[2] Institute of Edible Mushroom, Fujian Academy of Agricultural Sciences, Fuzhou 350012, China; kzh10@163.com
[3] Fujian Institute of Microbiology, Fuzhou 350007, China
[4] Institute of Integrative Medicine, Fujian University of Traditional Chinese Medicine, Fuzhou 350122, China
* Correspondence: photohost@126.com
† These authors contributed equally to this work.

Abstract

The fermentation endpoint of *Lactiplantibacillus plantarum*-fermented *Sparassis latifolia* superfine powder (SLSP) was defined in this study by integrating fermentation kinetics, electronic nose (E-nose), GC-IMS, GC×GC-TOFMS, non-targeted LC-MS, and electronic tongue (E-tongue) across six time points (0, 12, 24, 48, 72, and 96 h) of fermentation. Viable counts peaked at 24 h and then entered stationary phase; pH stabilized by 24 h, titratable acidity plateaued by 48 h, and reducing sugars were largely depleted by 48 h. E-nose identified 72 h as the key flavor-transition node; GC-IMS revealed a volatile profile shifting from fruity-grassy to nutty and wine-like notes before sulfur- and roast-derived off-notes emerged at 96 h. GC×GC-TOFMS further showed that total volatile content peaked at 72 h, and *rOAV* analysis confirmed that all 24 odor-active compounds exhibited *rOAV* ≥ 1 at 72 h, with the overall aroma intensity peaking at this stage, dominated by 1-octen-3-one. Non-targeted LC-MS resolved 334 metabolites into six temporal clusters, revealing that lipid oxidation products associated with flavor compound biosynthesis peaked at F72, while amino acid and fatty acid pools were progressively depleted. The E-tongue revealed no further significant taste improvement between 72 h and 96 h. Correlation analysis revealed a temporal coupling between polyunsaturated fatty acid depletion, lipid-oxidation products, and green/fatty aldehydes and ethyl esters, consistent with an LOX-type lipid-oxidation pathway; however, this interpretation remains correlative and would require enzyme activity or isotope-tracer evidence to be confirmed. These results provide a kinetic, metabolomic and sensory basis for defining 72 h as the fermentation endpoint of *Lp. plantarum*-fermented SLSP, replacing empirically determined fermentation time in industrial production.

Keywords: *Sparassis latifolia*; *Lactiplantibacillus plantarum*; fermentation endpoint; volatile flavor compounds; relative odor activity value; non-targeted metabolomics; solid-state fermentation

Check for updates

Academic Editors: Cristina Ghinea, Ana Leahu and Maria Soledad Prats Moya

Received: 16 October 2026
Revised: 10 November 2026
Accepted: 11 November 2026
Published: 13 November 2026

Copyright: © 2026 by the authors. Licensee MDPI, Basel, Switzerland. This article is an open access article distributed under the terms and conditions of the Creative Commons Attribution (CC BY) license.

1. Introduction

Edible mushrooms are increasingly exploited as functional food ingredients owing to their nutritional value and characteristic taste profile. *Sparassis latifolia* (*S. latifolia*) is an edible and medicinal fungus with high nutritional value and a distinctive texture [1,2], yet

the market is currently dominated by the fresh form, which is associated with a short shelf life and limited distribution channels. Processing of this fungus has been largely restricted to dried products, resulting in a narrow product range and limited added value. Broader processing strategies are therefore needed to expand the utilization of *S. latifolia*.

However, fresh *S. latifolia* possesses a dense texture and a complex cell-wall polysaccharide architecture [3], which hampers its fermentation. Ultrafine grinding (UG), a physical pretreatment that reduces particle size to the micrometer or even nanometer scale, disrupts cell wall integrity and promotes the release of intracellular components [4]. UG improves the extraction efficiency of water-soluble polysaccharides and phenolic compounds and enhances the release of free amino acids [5,6], thereby creating favorable conditions for subsequent microbial fermentation.

Microbial fermentation has drawn extensive attention for improving the nutrition, flavor, and bioactivity of foods, and lactic acid bacteria (LAB) fermentation represents a safe and mature bioprocessing strategy. Venugopal et al. [7] showed that LAB fermentation of *Lactarius deliciosus* yielded a product rich in phenols, indoles, and glucans, and Ayar-Sümer et al. [8] reported that LAB fermentation significantly increased the total phenolic content of mushrooms. Among LAB strains, *Lactiplantibacillus plantarum* (*Lp. plantarum*) is particularly well suited for this purpose: it exhibits broad substrate adaptability and strong tolerance to adverse conditions such as low pH and bile salts [9] and efficiently degrades macromolecules into small peptides, free amino acids, organic acids, and volatile flavor compounds (VFCs) [10]. In mushrooms such as shiitake (Lentinula edodes) and king oyster mushroom (*Pleurotus eryngii*), fermentation with *Lp. plantarum* significantly enhances umami intensity and aroma complexity [11]. In industrial practice, LAB fermentation is conventionally monitored through kinetic indicators, including pH, titratable acidity (TA), viable cell counts, and residual reducing sugars, which track microbial growth and acidification [12]. These kinetic parameters, however, describe how fermentation proceeds but not when the product smells and tastes best.

To bridge this gap, systematic characterization of flavor evolution calls for a multi-platform analytical approach. Electronic nose (E-nose) rapidly captures the overall volatile odor fingerprint of a sample through a pattern-recognition algorithm applied to a cross-reactive sensor array [13]. Gas chromatography-ion mobility spectrometry (GC-IMS) rapidly separates volatile components by both retention time and drift time, allowing the discrimination of volatile changes during fermentation [14]. Comprehensive two-dimensional gas chromatography-time-of-flight mass spectrometry (GC×GC-TOFMS) provides high-resolution separation and sensitivity, enabling both identification and quantification of VFCs in complex food matrices [15]. On the taste side, electronic tongue (E-tongue) is a high-throughput analytical technology that mimics human gustatory perception and enables objective, quantitative assessment of basic taste attributes, including sourness, sweetness, bitterness, saltiness, umami, and astringency [16]. Non-targeted liquid chromatography-mass spectrometry (LC-MS) tracks dynamic changes in non-volatile flavor-related metabolites, including peptides, lipids, and their precursors, and thereby provides biochemical insight into flavor development [17].

Despite these methodological advances, few studies have integrated ultrafine pulverization with *Lp. plantarum* fermentation to systematically resolve flavor-related metabolic changes in *S. latifolia*. More importantly, there is currently no clear definition of the fermentation endpoint for this substrate, i.e., the point where aroma-active metabolite accumulation ceases and substrate depletion begins. Kinetic indicators alone cannot locate this stage, because acidification and viable counts typically plateau before or after the flavor optimum [18,19]; flavor profiling alone, in turn, does not anchor the endpoint to the fermentation process. Without such a definition, processing risks either terminating fermen-

tation prematurely, leaving the flavor potential unrealized, or extending it unnecessarily, promoting the buildup of undesirable sulfur- and roast-derived off-notes. It is therefore essential to combine fermentation kinetics with multi-platform flavor metabolomics to identify the stage at which flavor-related metabolite accumulation reaches its maximum in *Lp. plantarum*-fermented *S. latifolia* superfine powder (SLSP). Accordingly, this study integrates E-nose, GC-IMS, GC×GC-TOFMS, E-tongue, and non-targeted LC-MS with parallel monitoring of pH, TA, viable counts, and reducing sugars to characterize the time-resolved remodeling of flavor and its precursors during *Lp. plantarum* fermentation of SLSP and to define the fermentation endpoint on metabolic evidence. The results are expected to provide a transferable, instrument-based criterion for terminating mushroom solid-state fermentation, replacing the conventional practice of fixed fermentation time and thereby reducing batch-to-batch flavor variability in the industry.

2. Materials and Methods

2.1. Materials

SLSP was provided by Fujian Tianyi Edible Fungi Co., Ltd. (Sanming, China), with a particle size of D90 ≤ 20 μm and a moisture content of ≤8%. *Lp. plantarum* strain SCLP-8, isolated in our laboratory and preserved in the China General Microbiological Culture Collection Center (accession number: CGMCC No. 29380), was used throughout this study.

N-hexyl-d_{13} alcohol (98.5%) and 2-amino-3-(2-chlorophenyl) propionic acid (98%) were purchased from C/D/N Isotopes Inc. (Pointe-Claire, QC, Canada) and TCI (Shanghai, China), respectively. 2-Methyl-3-heptanone (99.5%), an n-alkane series (C7–C40, 98%), and an n-ketone series (C4–C9, 98%) were obtained from Sigma-Aldrich (St. Louis, MO, USA). Acetonitrile (99.9%), formic acid, and ammonium formate (99.9%) were from Fisher Scientific (Loughborough, UK) and Sigma-Aldrich (Shanghai, China). 3,5-Dinitrosalicylic acid (DNS, ≥ 98%) was purchased from Aladdin (Shanghai, China). All other reagents and solvents were of analytical or chromatographic grade.

2.2. Sample Preparation and Fermentation Treatment

SLSP (50 g) was spread evenly in a ceramic dish to a layer thickness of approximately 3–4 mm. The sample was microwaved at 700 W for 30 s, with a 5-min interval, for a total of four cycles. The core temperature was measured using a food core temperature probe (Testo 104, Testo SE & Co. KGaA, Titisee-Neustadt, Germany; calibrated with a reference thermometer) inserted horizontally into the geometric center of the sample layer and was confirmed to reach 71.5 °C. After microwave treatment, the sample was examined for aerobic plate count according to the *National Food Safety Standard: Food Microbiological Examination: Aerobic Plate Count* (GB 4789.2-2022). After incubation at 36 ± 1 °C for 48 ± 2 h, no colonies were observed, indicating that the microwave treatment achieved effective microbial inactivation. The sterilized SLSP was then aseptically dispensed into individual sterile polypropylene containers at 10 g per container prior to inoculation.

Lp. plantarum was inoculated into MRS broth and incubated at 37 °C for 12 h. The strain was subcultured two to three times in MRS broth prior to use. Cells were harvested by centrifugation (5000 rpm, 5 min), washed three times with sterile normal saline to remove residual medium components, and resuspended. McFarland standards were used for rapid turbidity matching to adjust the bacterial suspension to a cell density of 7.00 log CFU/mL. Immediately after adjustment, viable cell enumeration of the inoculum suspension was performed according to the *National food safety standard-Food microbiological examination-Examination of lactic acid bacteria* (GB 4789.35-2023). Briefly, 25 mL of the inoculum suspension was mixed with 225 mL of tryptone-saline diluent under aseptic conditions to prepare a 1:10 initial suspension. Serial ten-fold dilutions were performed to

obtain 10^{-1} to 10^{-6} sample suspensions. Aliquots (1 mL) of 10^{-5} and 10^{-6} dilutions were pour-plated onto MRS agar (48–50 °C). After agar solidification, plates were incubated anaerobically at 36 ± 1 °C for 48 ± 2 h. Plates with colony counts between 30 and 300 were selected for enumeration. The actual inoculation dosage was calculated based on the measured viable cell count of the inoculum suspension. For each fermentation container, 10 mL of the adjusted bacterial suspension (7.00 log CFU/mL) was inoculated into 10 g of sterilized SLSP, giving a 1:1 (v/w) inoculum-to-substrate ratio and an initial inoculation dose of approximately 7.0 log CFU/g substrate.

All treatments were arranged in a completely randomized design. The experiment included six fermentation time points (0 h, 12 h, 24 h, 48 h, 72 h, and 96 h), designated as UF, F12, F24, F48, F72, and F96, respectively (Figure 1). UF served as the unfermented control, referring to the sample taken immediately after inoculation (0 h) before any detectable fermentation occurred. A sterilized, non-inoculated control incubated in parallel was not included in the experimental design, which is acknowledged as a methodological constraint. For each time point, independent fermentation units were established to ensure sufficient sample availability for subsequent analyses. Three independent biological replicates were harvested for each group. After inoculation, all samples were simultaneously placed in a constant-temperature incubator and fermented statically at 37 °C. At each sampling point, samples were immediately removed to halt fermentation and stored at −80 °C until multi-platform detection. All analytical aliquots were weighed on a fresh-weight basis.

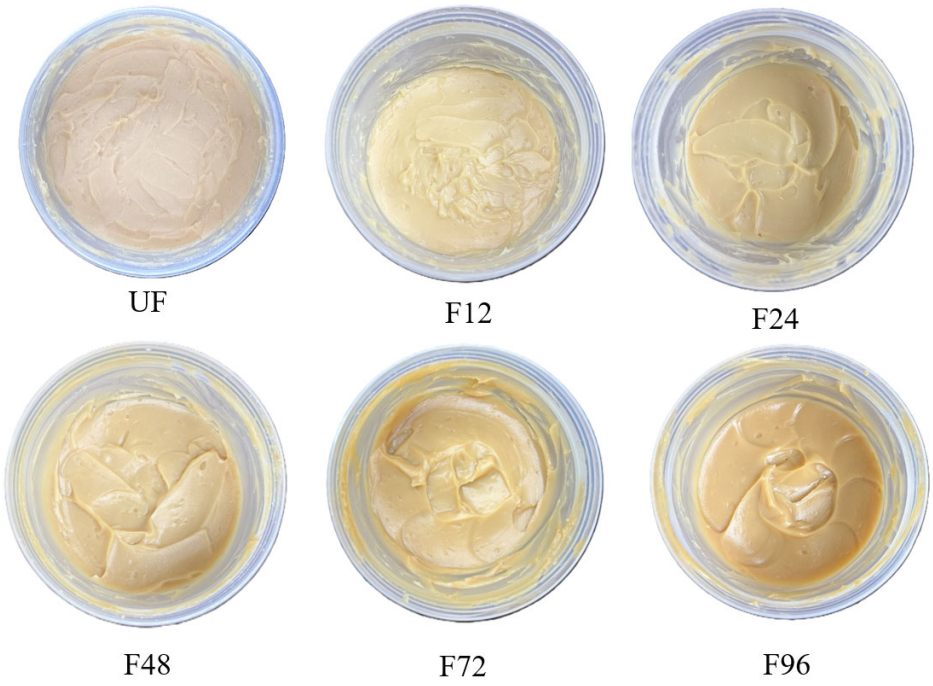


Figure 1. Six fermentation stages of SLSP: UF, F12, F24, F48, F72, and F96.

2.3. Physicochemical and Microbiological Properties

2.3.1. pH and TA

An accurately weighed 5.00 g aliquot of each sample was homogenized with 45 mL of CO_2-free distilled water, and the pH of the resulting suspension was measured with a calibrated pH meter (STARTER3C, OHAUS Corporation, Parsippany, NJ, USA). TA was determined according to the *National Food Safety Standard: Determination of Total Acid in Foods* (GB 12456-2021). Because each individual fermentation container contained only 10 g of SLSP, which was insufficient for the 25 g sample required by GB 12456-2021, containers from the same independent biological replicate were aseptically pooled and homogenized

to obtain a composite sample of sufficient mass for TA extraction. TA was then measured once for each of the three independent biological replicates ($n = 3$). Briefly, 25 g of homogenized sample was extracted with CO_2-free hot water (80 °C) in a boiling water bath for 30 min. After cooling, the extract was volumetrically adjusted, filtered, and titrated potentiometrically with 0.1 mol/L NaOH. TA was expressed as the neutralization capacity in mmol NaOH/kg of sample as Equation (1).

$$X = \frac{(V_1 - V_0) \times c \times 1000}{\mathrm{m}} \quad (1)$$

V_0, volumes consumed by reagent blank, mL; V_1, volumes consumed by the sample, mL; c, the concentration of NaOH (0.1 mol/L); m, the sample mass, g. For comparison with values reported as lactic acid equivalents, TA in mmol NaOH/kg can be converted by multiplying by 0.09008 (g/mmol).

2.3.2. Enumeration of *Lp. plantarum*

For enumeration of *Lp. plantarum* in solid-state fermentation samples: under aseptic conditions, 10 g of sample was taken from each independent fermentation vessel and mixed with 90 mL of peptone saline diluent to prepare a 1:10 primary homogenate. Subsequent operations were performed following GB 4789.35-2023.

2.3.3. Determination of Reducing Sugar

Reducing sugars were determined by the 3,5-dinitrosalicylic acid (DNS) method [20]. Briefly, an accurately weighed 1.00 g aliquot of each sample was extracted with 10 mL of distilled water at 60 °C for 30 min and centrifuged (12,000× *g*, 10 min). An aliquot (1.0 mL) of the supernatant was mixed with 1.0 mL of DNS reagent, heated in a boiling water bath for 5 min, and immediately cooled in an ice-water bath. After dilution to 10 mL with distilled water, the absorbance was measured at 540 nm against a blank, and the reducing sugar content was calculated from a glucose standard curve (0–2.0 mg/mL) and expressed as g/100 g (glucose equivalents).

2.4. Aroma and Taste Analysis

2.4.1. E-Nose Analysis

The samples were subjected to E-nose analysis using the PEN3 E-nose system from Airsense Analytics GmbH (Schwerin, Germany). Exactly 1.00 g of the sample was placed in a 15 mL headspace vial, sealed, and equilibrated for at least 30 min before analysis. The E-nose comprises a total of ten metal oxide gas sensors, each specializing in detecting different compounds (W1C for aromatics, W5S for nitrogen oxides, W3C for ammonia and aromatics, W6S for hydrogen, W5C for alkanes and aromatics, W1S for methane, W1W for sulfides, W2S for alcohols, W2W for organic sulfur, and finally, W3S for alkanes). The analysis program was as follows: sensor preconditioning (self-cleaning: 120 s, zeroing: 5 s) and sample preparation (5 s) were performed, followed by a 120-s analytical phase at a constant flow rate of 300 mL/min, with the collected sensor signals utilized for subsequent analysis.

2.4.2. GC-IMS Analysis

GC-IMS analysis was performed using a FlavorSpec® instrument (G.A.S., Dortmund, Germany) equipped with an MXT-5 capillary column (15 m × 0.53 mm × 1.0 µm; Restek, Bellefonte, PA, USA). The samples (2.00 g) were accurately weighed into a 20 mL headspace vial, followed by the addition of 10 µL of internal standard (2-methyl-3-heptanone, 100 µg/mL). The vial was incubated at 60 °C for 20 min with agitation at 500

r/min, after which 500 µL of the headspace gas was injected in splitless mode. The injection needle temperature was maintained at 85 °C. The programmed carrier gas flow (99.999% pure nitrogen) was set to an initial flow rate of 2 mL/min for 2 min and ramped to 10 mL/min within 8 min, then ramped to 100 mL/min within 10 min, and the whole run time was 20 min. The IMS was set at 45 °C and operated in positive ion mode.

2.4.3. GC×GC-TOFMS Analysis

A 0.50 g aliquot of the sample was precisely weighed into a 20 mL headspace vial, followed by the addition of 10 µL of an internal standard solution containing N-hexyl-d_{13} alcohol (10 µg/mL). The prepared vial was then incubated at 80 °C for 10 min (30/60 µm DVB/CAR fiber, Supelco, Bellefonte, PA, USA). Before extraction, the SPME fiber was conditioned in the GC injection port at 270 °C for 10 min. The conditioned fiber was subsequently inserted into the vial headspace and exposed at 80 °C for 25 min. Upon completion of adsorption, the fiber was transferred to the GC injection port, where thermal desorption was performed at 250 °C for 5 min. Finally, the fiber was reconditioned at 270 °C for 10 min before subsequent use. For system performance monitoring, a separate 10 µL aliquot of n-alkane standard was processed in parallel using the same incubation, extraction, and injection procedure.

Analyses were carried out using a LECO Pegasus® 4D instrument (LECO, St. Joseph, MI, USA) consisting of an Agilent 8890A GC (Agilent Technologies, Palo Alto, CA, USA). The system was equipped with a split/splitless injector and a dual-stage cryogenic modulatorcoupled with a TOFMS detector (LECO, St. Joseph, MI, USA). A DB-Wax (30 m × 250 µm I.D., 0.5 µm) (Agilent, Santa Clara, CA, USA) was used as a first-dimension column (1D), and Rxi-5Sil MS (2.0 m × 150 µm I.D., 0.15 µm) (Restek, Bellefonte, PA, USA) was used as a second-dimension column (2D). The carrier gas was high-purity helium (>99.999%) at a constant flow rate of 1.0 mL/min. The oven temperature program was as follows: held at 50 °C for 2 min, increased to 230 °C at 5 °C/min, and held for 5 min. The secondary oven temperature was operated at 5 °C higher than the first oven. The temperature setting for the modulator was always 15 °C higher than that of the secondary oven. The modulator was operated with a 6.0 s modulation period. The GC injector temperature was 250 °C.

The transfer line and ion source temperatures were both set at 250 °C. The acquisition frequency was 200 spectra/s. The mass spectrometer was operated in the EI mode at 70 eV with a range of m/z 35–550 and detector voltage of 1960 V.

2.4.4. Calculation of Relative Odor Activity Value (*rOAV*)

The internal standard (*N*-hexyl-d_{13} alcohol) semi-quantitative method was used to calculate the relative metabolite contents as Equation (2):

$$X_i = \frac{V_s \times C_s \times I_i}{M \times I_s} \quad (2)$$

X_i, Analyte concentration, µg/kg; V_s, Volume of internal standard, µL; C_s, Internal standard concentration, µg/µL; I_i, Peak area of the analyte; I_s, Peak area of the internal standard; M, Sample mass, g.

rOAV analysis: *rOAV*s were calculated using Equation (3)

$$rOAV = \frac{X_i}{T_i} \quad (3)$$

X_i, Analyte concentration, µg/kg; T_i, Odor threshold, µg/kg.

The *OTi* (odor threshold) values were taken from the compilation of van Gemert [21], using the thresholds reported in water. Compounds with $rOAV \geq 1$ were provisionally classified as odor-active; given the semi-quantitative nature of X_i, *rOAV* values should be

interpreted as a relative ranking of aroma contribution rather than as an absolute measure of odor intensity.

2.4.5. E-Tongue Analysis

An E-tongue, equipped with the Taste-Sensing System SA 402B (Intelligent Sensor Technology, Inc., Atsugi, Japan), was used to characterize the samples' taste profile. The electronic tongue contains seven sensitive electrodes, which are sensitive to sourness, bitterness, astringency, umami, richness, saltiness, and sweetness, respectively.

The sample was homogenized with ultrapure water at a solid-to-liquid ratio of 1:10 (w/v). The homogenate was then ultrasonicated for 10 min and filtered through a 0.22-μm nylon membrane. The resulting supernatant was collected for subsequent analysis. Because the E-tongue measurement requires a liquid phase, the taste profile reflects the water-extractable taste-active compounds recovered by the 1:10 (w/v) extraction; non-extractable matrix-bound or lipid-soluble components are not captured by this method. The measurement procedure was performed as follows: first, the sensor was immersed in positive and negative cleaning solutions for 90 s each, followed by two 120 s rinses in different reference solutions. After returning to the equilibrium position for 30 s, the sensor initiated a 30 s detection phase.

2.5. Non-Targeted Metabolomics Profiling Using LC-MS

An accurate amount of 0.03 g of sample was weighed into a 2 mL centrifuge tube, followed by the addition of 100 mg of glass beads and 1 mL of 50% aqueous methanol. The mixture was vortexed for 30 s, then placed in a 2 mL adapter compatible with the tissue grinder and rapidly frozen in liquid nitrogen for 5 min. After thawing at room temperature, the tube was reinserted into the adapter and ground at 55 Hz for 2 min. This freeze–thaw–grind was repeated twice. Subsequently, the sample was centrifuged (12,000× g, 4 °C, 10 min), and the entire supernatant was transferred to a new 2 mL centrifuge tube, then concentrated and dried under vacuum. The residue was accurately reconstituted with 300 μL of 50% aqueous methanol containing 2-amino-3-(2-chlorophenyl) propionic acid as an internal standard, filtered through a 0.22 μm membrane, and transferred into an autosampler vial for LC-MS analysis.

The LC analysis was performed on a Vanquish UHPLC System (Thermo Fisher Scientific, Waltham, MA, USA). Chromatography was performed on an ACQUITY UPLC® HSS T3 (2.1 × 100 mm, 1.8 μm) (Waters, Milford, MA, USA). The column was maintained at 40 °C. The flow rate and injection volume were set at 0.3 mL/min and 2 μL, respectively. For LC-ESI (+)-MS analysis, the mobile phases consisted of (B2) 0.1% formic acid in acetonitrile (v/v) and (A2) 0.1% formic acid in water (v/v). Separation was conducted under the following gradient: 0~1 min, 10% B2; 1~5 min, 10~98% B2; 5~6.5 min, 98% B2; 6.5~6.6 min, 98~10% B2; 6.6~8 min, 10% B2. For LC-ESI (-)-MS analysis, the analytes were eluted with (B3) acetonitrile and (A3) ammonium formate (5 mM). Separation was conducted under the following gradient: 0~1 min,10% B3;1~5 min,10~98% B3; 5~6.5 min,98% B3; 6.5~6.6 min, 98~10% B3; 6.6~8 min, 10% B3.

Mass spectrometric detection of metabolites was performed on an Orbitrap Exploris 120 (Thermo Fisher Scientific, Waltham, MA, USA) with an ESI ion source. Simultaneous MS1 and MS/MS (Full MS-ddMS2 mode, data-dependent MS/MS) acquisition was used. The parameters were as follows: sheath gas pressure, 40 arb; aux gas flow, 10 arb; spray voltage, 3.50 kV and −2.50 kV for ESI(+) and ESI(−), respectively; capillary temperature, 325 °C; MS1 range, m/z 100–1000; MS1 resolving power, 60000 FWHM; number of data-dependent scans per cycle, 4; MS/MS resolving power, 15000 FWHM; normalized collision energy, 30%; dynamic exclusion time, automatic.

2.6. Statistical Analysis

All analyses were performed on three independent biological replicates per fermentation stage, and results are expressed as mean ± standard deviation. Normality and homogeneity of variance of each dataset were assessed using the Shapiro–Wilk and Levene tests, respectively. Where these assumptions were satisfied, differences among fermentation stages were evaluated by one-way analysis of variance (ANOVA) followed by Tukey's HSD test; otherwise, the Kruskal–Wallis test with Dunn's post hoc comparisons was applied. Multiple testing was controlled using the Benjamini–Hochberg false discovery rate, with adjusted p-values (<0.05) considered significant.

Principal component analysis (PCA) was used for exploratory analysis without supervised grouping. Orthogonal partial least squares discriminant analysis (OPLS-DA) was applied to maximize group separation, and model reliability was evaluated by 200-permutation tests of the Y-labels together with cross-validated analysis of variance (CV-ANOVA). Volatile compounds with variable importance in projection (VIP) ≥ 1.0 were first retained as differential compounds; among these, the compounds significantly upregulated in each fermented group relative to UF were further screened by the criteria of $|\log_2 FC| \geq 1$ and $p < 0.05$ using volcano plots. *rOAV*s were compared among stages by Kruskal–Wallis tests with Dunn's post hoc test.

Compounds were identified as follows. For GC-IMS, retention indices (RI) were calculated using n-ketones (C4–C9) and matched against a commercial database (G.A.S., Dortmund, Germany) together with drift times; fingerprints were generated with the Gallery Plot plugin in VOCal. For GC×GC-TOFMS, the first-dimension RI was derived from a parallel n-alkane series (C7–C40) using the Van den Dool and Kratz equation; tentative identification combined RI tolerance (<30 units) and spectral similarity (≥ 800) against the NIST and Wiley libraries, with semi-quantification against N-hexyl-d_{13} alcohol. For LC-MS, peak detection, retention-time alignment, and grouping were performed with XCMS using centWave peak picking. Metabolites were annotated by multi-library MS/MS spectral matching, with confirmation by mass error < 5 ppm, molecular formula, and adduct ion validation. Relative quantification was performed by normalizing each compound's signal to that of the internal standard, followed by total-peak-area normalization to correct for systematic drift. Annotation confidence levels were assigned according to the Metabolomics Standards Initiative (MSI): Level 1, metabolites matched against an in-house authentic-standard MS/MS spectral library (BioDeepDB) with m/z error < 5 ppm; Level 2, metabolites putatively annotated by MS/MS spectral matching to public databases (mzCloud, MoNA, METLIN, HMDB) or predicted spectra (DeepMS); Level 3, metabolites putatively characterized based on physicochemical properties (m/z, retention time) using retention-time prediction (MetaDNA) or library matching without MS/MS confirmation.

Unsupervised k-means clustering of the standardized temporal metabolite profiles resolved accumulation patterns, with k selected by the Calinski-Harabasz index ($n = 334$). Spearman correlations among VFCs ($rOAV \geq 1$) and representative non-volatile metabolites from the six subclusters were computed on all 18 individual samples (6 stages × 3 replicates) after $\log_2(x + 1)$ transformation; significance was defined as $|\rho| > 0.7$ with BH-adjusted $p < 0.05$.

Statistical analysis and graphics were performed using SIMCA 14.1 (PCA/OPLS-DA), SPSS 26.0 (ANOVA), OriginPro 2023, and Metware Cloud (https://cloud.metware.cn).

3. Results and Discussion

3.1. Fermentation Kinetics and Physicochemical Changes

The growth and metabolic activity of *Lp. plantarum* during SLSP fermentation were characterized by measuring pH, TA, viable cell counts, and reducing sugar content across the six fermentation stages (Figure 2).

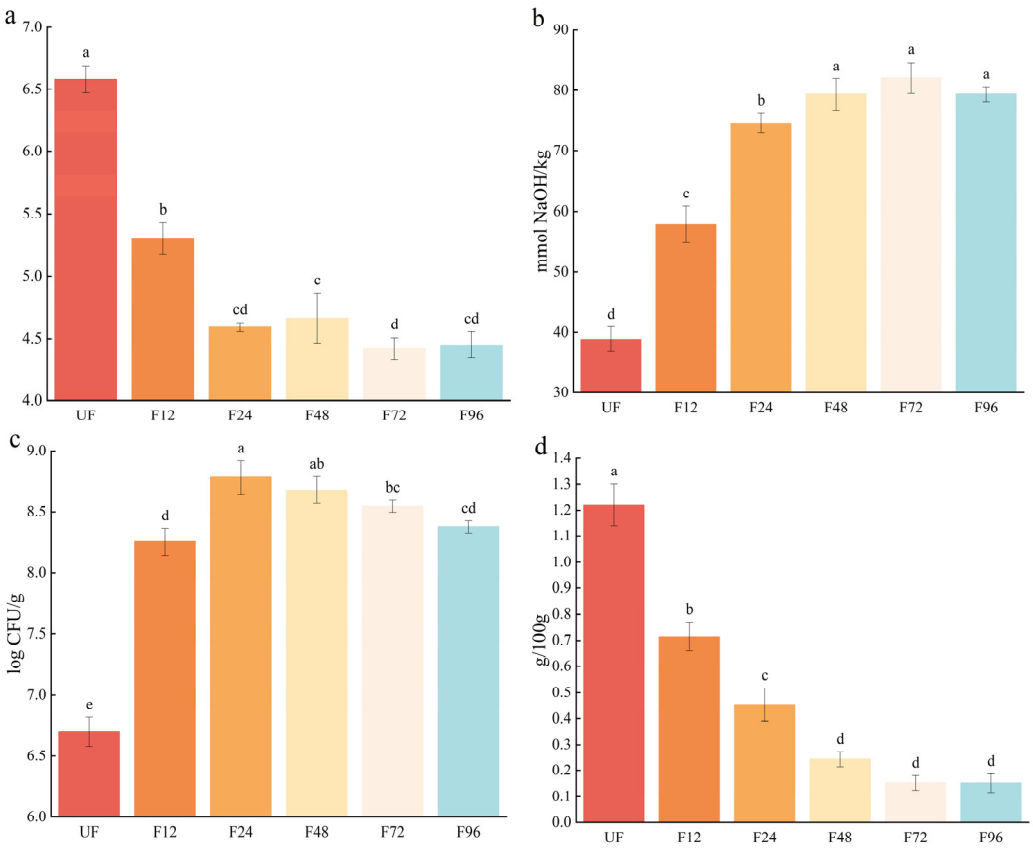


Figure 2. Fermentation kinetics of *Lp. plantarum*-fermented SLSP. (**a**) pH. (**b**) TA (mmol NaOH/kg). (**c**) viable cell counts (log CFU/g). (**d**) reducing sugar content (g/100 g). Error bars indicate standard deviation from mean values ($n = 3$), and different lowercase letters indicate significant differences between means ($p < 0.05$).

As shown in Figure 2a, the pH value dropped rapidly within the first 24 h and then stabilized in a relatively low and narrow range. The decline was more pronounced in the early stage: the pH decreased significantly from the unfermented state to 12 h and continued to fall by 24 h. From 24 h onward, the pH remained relatively stable, fluctuating between 4.4 and 4.7, indicating that most acid production occurred within the first day of fermentation. The changes in TA corresponded to those in pH (Figure 2b). TA increased continuously over the first 48 h and then reached a plateau. The rise was faster during the first 24 h and slowed thereafter, with no significant increase observed between 48 and 96 h.

Viable cell counts followed a typical bacterial growth curve (Figure 2c). The counts rose rapidly from the baseline level of the unfermented sample, peaked at 24 h, and then entered a stationary phase that lasted until 48 h. Afterwards, the counts gradually declined, which was likely due to the low pH and reduced substrate availability.

Reducing sugar content decreased continuously throughout fermentation (Figure 2d). The decline was fastest during the first 24 h, reflecting rapid sugar consumption during the exponential growth phase. By 48 h, reducing sugars had fallen to a low level, with no further significant decrease at later stages. The timing of near sugar exhaustion roughly

coincided with the onset of the decline in viable cell counts from their peak, suggesting that insufficient carbon source became the main factor limiting further cell growth after 48 h.

Collectively, the profiles of pH, TA, viable cell counts, and reducing sugars indicate that the most active growth and acid production occurred within the first 24 h, followed by a gradual decline in metabolic activity after 48 h due to the depletion of fermentable sugars. The period from 48 to 72 h therefore represents a transition stage in which primary fermentation activity had largely subsided and the system approached a relatively stable state.

3.2. E-Nose

The volatile odor fingerprints of the sample at different fermentation stages were analyzed by E-nose, and the PCA results are shown in Figure 3a. PC1 and PC2 accounted for 70.6% and 26.2% of the total variance, respectively (cumulative 96.8%); the PCA model yielded $R^2X(cum) = 0.995$ and $Q^2(cum) = 0.970$. Samples from the same fermentation time were tightly clustered, while those from different time points were clearly distinguished. The odor profiles changed distinctly across fermentation stages, revealing that fermentation duration strongly reshaped overall odor fingerprints.

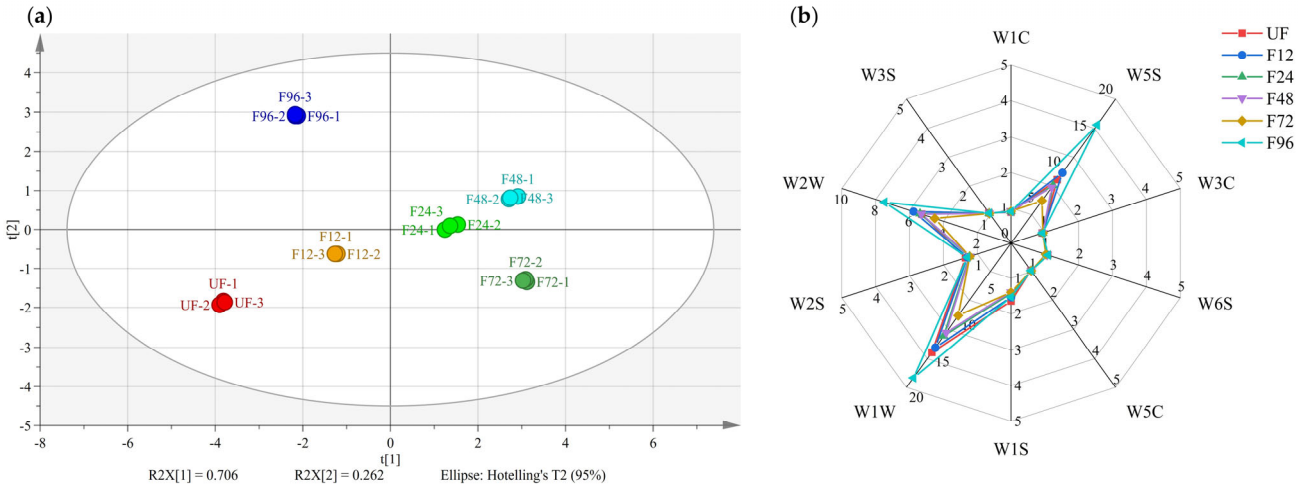


Figure 3. Olfactory characterization of six fermentation stages (UF, F12, F24, F48, F72, F96). (**a**) E-nose PCA plot. (**b**) E-nose radar chart.

As shown in Figure 3b, sensors W1W, W2W, and W5S exhibited the most pronounced changes. W1W and W2W are associated with volatile sulfur compounds (VSCs). W1W continuously decreased from UF to F72, whereas W2W briefly increased before dropping to its lowest point at F72. This indicates that the unfermented SLSP contains a relatively high level of VSCs. From F72 to F96, the response values of both W1W and W2W rose sharply, suggesting that *Lp. plantarum* extensively degraded sulfur-containing proteins and sulfur flavor precursors in SLSP during this period, leading to substantial release of VSCs. Rajendran et al. [17] reported that *Lp. plantarum* can metabolize methionine to generate VSCs. The W5S sensor, which reflects changes in nitrogen oxides, decreased continuously from UF to 72 h and then increased sharply from 72 to 96 h. The continuous decline in early fermentation implied progressive consumption of nitrogenous substrates for microbial growth, whereas the later increase mainly reflected the accumulation of nitrogen-containing heterocyclic volatiles (e.g., pyrazines) associated with microbial amino-acid catabolism and subsequent condensation reactions, as supported by the GC×GC-TOFMS data. In addition, the W1S and W2S sensors exhibited their highest responses in the UF sample, which decreased slightly as fermentation progressed. Meanwhile, the W1C, W3C, W5C,

W3S, and W6S sensors showed no significant changes across different fermentation stages. Overall, fermentation significantly altered the odor profile of SLSP, and marked differences in multiple volatile components were observed between F72 and F96, further indicating that 72 h is a critical time point for flavor transition.

3.3. GC-IMS

A total of 67 VFCs corresponding to 86 peaks, including monomers and dimers, were identified across all samples (Figure 4). These compounds were classified into nine categories: 18 aldehydes, 14 alcohols, 11 ketones, 9 heterocyclic compounds, 7 esters, 3 VSCs, 2 acids, 2 aromatic hydrocarbons, and 1 alkene. The relative contents of acids, alcohols, aldehydes, esters, heterocyclic compounds, and ketones dominated the overall volatile profile, with acids and alcohols peaking early and heterocyclic compounds rising in later stages.

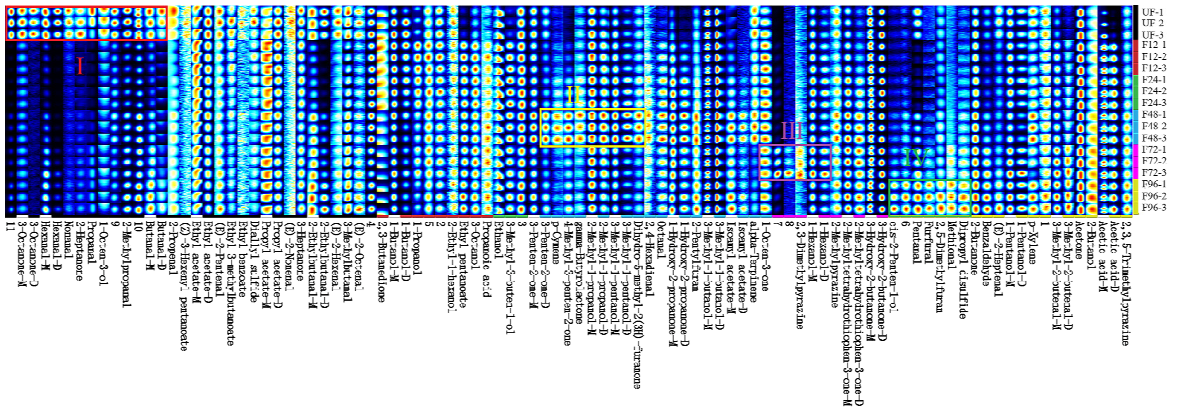


Figure 4. GC-IMS Fingerprints of six fermentation stages (UF, F12, F24, F48, F72, F96). The color gradient represents the signal intensity of volatile compounds: blue indicates low intensity, and red indicates high intensity.

The fingerprint plot (Figure 4) revealed stage-specific compound patterns. Acetone and 3-hydroxy-2-butanone maintained relatively high concentrations throughout. In UF (Region I), several compounds remained at relatively high levels, including butanal (pungent, fruity, green leaf), 2-methylpropanal (banana, melon, slightly nutty), 1-octen-3-ol (mushroom, lavender, rose, hay), propanal (pungent, green grassy), 2-heptanone (pear, banana, fruity, slight medicinal fragrance), nonanal (rose, citrus, strong oily), hexanal (fresh, green, fat, fruity), and 3-octanone (mouldy, ketone, green, waxy, vegetable, mushroom, cheese, fruity). These compounds represent the major intrinsic flavor substances of SLSP, which were predominantly characterized by fruity, grassy, mushroom, and pungent notes. In F48 (Region II), several compounds were prominent, including dihydro-5-methyl-2(3*H*)-furanone (herbal, sweet, tobacco, woody), 3-methyl-1-pentanol (wine, cocoa, green, fruity), 2-methyl-1-propanol (fresh, alcoholic, leather), γ-butyrolactone (cream, fat, caramel), 4-methyl-3-penten-2-one (spice, earth, green), p-cymene (fresh, citrus terpene, woody, spice), and 3-penten-2-one (fruity, spicy). The flavor profile of this sample was predominantly characterized by sweet, herbal, woody, spicy, and creamy caramel notes. In F72 (Region III), 1-hexanol (fresh, fruity, wine, sweet, green) and 2,3-dimethylpyrazine (nutty) were relatively abundant, thereby highlighting nutty, fresh fruity, and wine-like notes. In F96 (Region IV), dipropyl disulfide (sulfury, onion), methional (onion, meat, fruity), 2,5-dimethylfuran (meaty, roast beef, bacon), furfural (sweet, woody, almond, bready), pentanal (green grassy, faint banana, pungent), and cis-2-penten-1-ol (green, plastic, rubber) exhibited higher concentrations. The elevated levels of VSCs aligned with the responses of E-nose sensors W1W

and W2W, driving an aroma profile characterized by intense meaty, sulfury, roasted, and plastic-like notes.

Taken together, the GC-IMS fingerprint resolved a time-dependent remodeling of the volatile profile across the six fermentation stages. Early fermentation (F12–F24) was dominated by a rapid surge of acids and alcohols, reflecting the vigorous primary metabolism of *Lp. plantarum*; by F48, heterocyclic compounds had accumulated to their plateau and the profile shifted toward sweet, herbal, and caramel-like notes. At F72, the concurrent enrichment of 1-hexanol and 2,3-dimethylpyrazine marked the transition toward a nutty, fresh-fruity, and wine-like aroma, whereas further extension to F96 introduced pronounced meaty, sulfury (dipropyl disulfide, methional), and roasted notes (2,5-dimethylfuran, furfural), alongside a plastic-like green character from cis-2-penten-1-ol. Thus, GC-IMS independently identified F72 as the inflection point at which the fruity/nutty aroma peaked and beyond which sulfur- and roast-derived off-notes began to emerge.

3.4. GC×GC-TOFMS

In contrast to the rapid and sensitive detection afforded by GC-IMS, GC×GC-TOFMS, owing to its higher resolution and sensitivity, enables more accurate and comprehensive identification of a greater number of compounds [22]. Table S1 lists the 264 VFCs identified by GC×GC-TOFMS, categorized into 44 esters, 36 aldehydes, 37 alcohols, 46 heterocyclic compounds, 23 ketones, 23 alkenes, 17 alkanes, 18 acids, 15 aromatic hydrocarbons, and 5 phenols. As shown in Figure 5a, F96 and F72 exhibited peak values in the number of VFCs and their total content, respectively. The total content of VFCs in all fermented groups (F12–F96) was significantly higher than that in UF, consistent with GC-IMS results. This indicates that *Lp. plantarum* fermentation promoted the generation of flavor-active substances effectively [23]. Notably, the total content of VFCs at F96 decreased significantly relative to F72. This suggests that 72 h is a critical window for maximal flavor accumulation in SLSP fermentation. Prolonged fermentation after 72 h fails to accumulate more aroma substances.

The OPLS-DA model, comprising three predictive and two orthogonal components, clearly separated the six fermentation stages along the predictive component (Figure 5b). The model yielded $R^2X(cum) = 0.840$, $R^2Y(cum) = 0.990$, and $Q^2(cum) = 0.958$, indicating good model fit and predictive ability. Per-Y-variable analysis confirmed that this performance was uniformly high across all six stages ($R^2Y(var) \geq 0.95$; $Q^2Y(var) \geq 0.93$), indicating that the separation was not driven by any single group. Model reliability was further confirmed by a 200-permutation test (R^2 intercept = 0.51, Q^2 intercept = −0.789) and CV-ANOVA ($p < 0.001$, $F = 21.11$); the negative Q^2 intercept and the significant CV-ANOVA p-value together demonstrate that the model was not overfitted and the group discrimination was not driven by random chance. As shown in Figure 5b, with the progression of fermentation, the groups underwent significant differentiation and exhibited a time-dependent dynamic trajectory. Subsequently, 136 VFCs with a VIP ≥ 1.0 were identified as differential compounds (Figure 5c). This indicates that significant shifts occur in the volatile metabolic profile during fermentation. Next, volcano plot analysis ($|\log_2 FC| \geq 1$ and $p < 0.05$) was applied to these 136 VIP ≥ 1.0 compounds to determine the VFCs that were significantly upregulated in each fermentation group relative to the UF. Specifically, the F12, F24, F48, F72, and F96 groups showed 21, 20, 21, 23, and 20 significantly upregulated VFCs, respectively (Figure 5d–h).

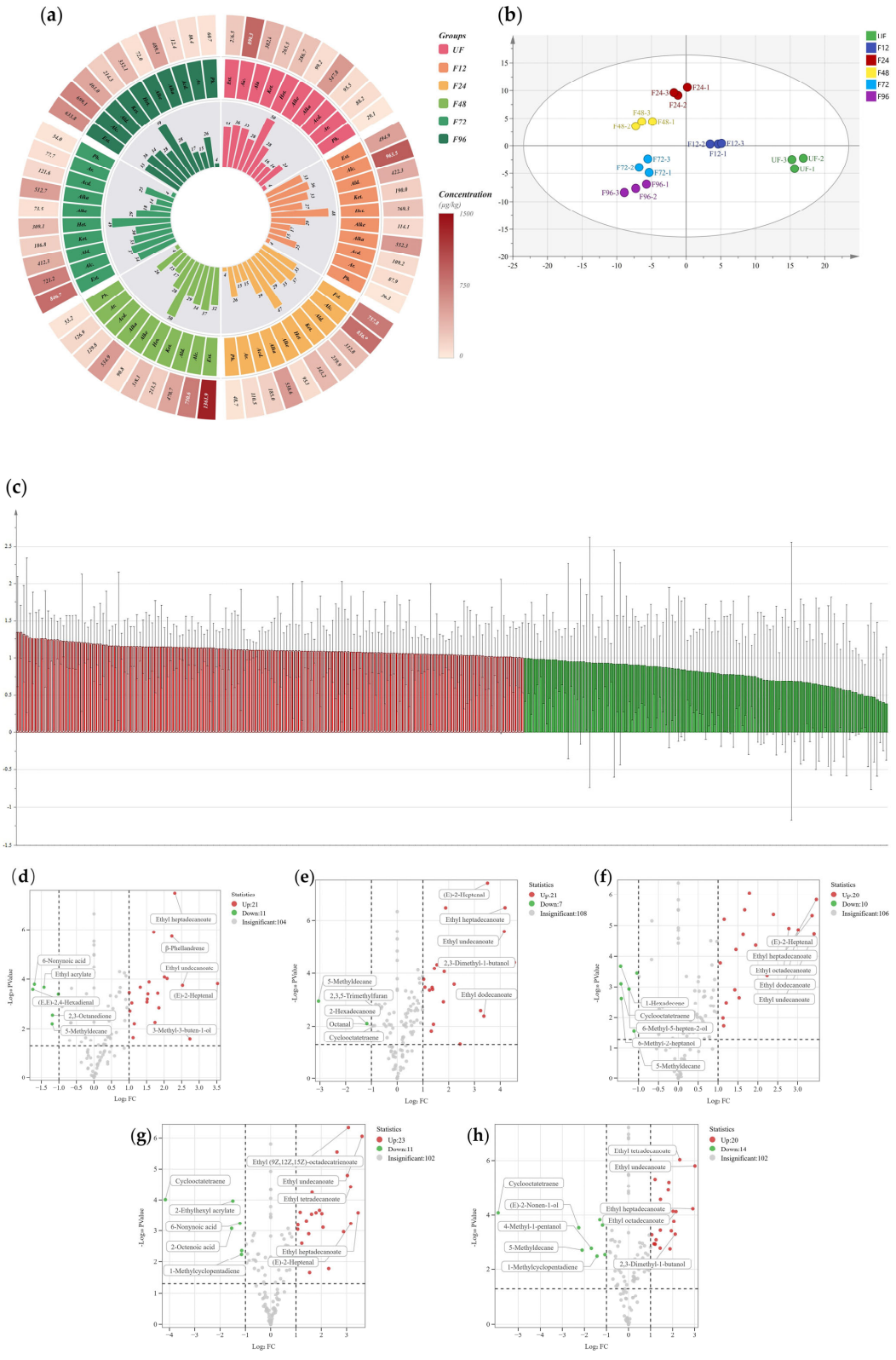


Figure 5. Dynamic changes in aroma compounds of six fermentation stages (UF, F12, F24, F48, F72, F96). (**a**) Numbers and total contents of VFCs across the six stages. (**b**) OPLS-DA. (**c**) Red bars denote compounds with VIP > 1.0 and green bars denote compounds with VIP ≤ 1.0. (**d**–**h**) Volcano plots comparing F12, F24, F48, F72, and F96 to UF, respectively.

3.4.1. Esters

Esters constituted the most abundant class of VFCs in fermented SLSP, accounting for >50% of total volatile content at F72 (Figure 5a), consistent with the GC-IMS observation of increasing fruity notes [24]. The high-resolution GC×GC-TOFMS platform further revealed a detailed ester profile comprising 44 individual compounds, with ethyl esters dominating. Specifically, ethyl heptadecanoate, ethyl undecanoate, ethyl tetradecanoate, ethyl octadecanoate, and ethyl (9*Z*,12*Z*,15*Z*)-octadecatrienoate increased markedly across fermentation, indicating continuous microbial esterification throughout the process. This substantial ester accumulation conferred rich fruity and sweet notes, harmonized the overall aroma, and helped mask potential off-odors [25]. The buildup of esters is generally attributed to esterification, in which free alcohols are converted to their corresponding esters [26], consistent with the decreasing alcohol content observed in both GC-IMS and GC×GC-TOFMS.

3.4.2. Alcohols

Alcohols ranked second only to esters in relative abundance among total VFCs. The alcohols detected in SLSP were predominantly short- to medium-chain (≤ C10), such as 2-octanol, 6-methyl-5-hepten-2-ol, 1-octanol, 3-methyl-2-butanol, and (*E*)-2-nonen-1-ol. These low-molecular-weight alcohols are highly volatile and possess low odor thresholds. During fermentation, their contents decreased significantly, reflecting the combined effects of several processes. First, they served as substrates for esterification; for example, 1-octanol reacts with acetic acid to yield octyl acetate, whereas ethanol is the precursor of ethyl acetate [27]. Second, *Lp. plantarum* can utilize alcohols as carbon sources, channeling them into the tricarboxylic acid (TCA) cycle via the acetyl-CoA pathway [28]. Third, alterations in precursor metabolism contributed: 6-methyl-5-hepten-2-ol is typically generated by oxidative cleavage of carotenoids, and the blockage of this biosynthetic route during fermentation, together with the compound's high volatility, further lowered its content.

3.4.3. Aldehydes

Aldehydes generally exhibit low odor thresholds [29] and contribute fruity, floral, and nutty aromas. Their contents increased significantly after fermentation, as exemplified by (*E*)-2-heptenal, (*E*, *E*)-2,4-octadienal, 2,4-nonadienal, pentanal, and 2-methylbutanal (Figure 5d–h). Lipid oxidative degradation and Strecker degradation of amino acids were the principal sources of these aldehydes [30]. (*E*)-2-heptenal rose significantly as early as F12 and remained elevated thereafter, indicating that lipid oxidation was activated in the initial fermentation phase. In addition, enzymatic oxidation of alcohols contributed to aldehyde formation: the primary alcohol 1-octanol is oxidized by alcohol dehydrogenase (ADH) to octanal [31]. Notably, the odd-numbered aldehydes detected here, including pentanal (C5), (*E*)-2-heptenal (C7), and 2,4-nonadienal (C9), are not de novo products of microbial fatty-acid biosynthesis, which yields only even-chain fatty acids; rather, they arise from the oxidative cleavage of substrate-derived C18 polyunsaturated fatty acids (linoleic and α-linolenic acids) at different positions of their hydroperoxide intermediates [32].

3.4.4. Acids

Acids showed a trend of first increasing and then decreasing, peaking at F24, consistent with the GC-IMS results. This pattern mainly reflects that, after fermentation initiation, *Lp. plantarum* extensively converted sugars into organic acids; in later stages, these acids were consumed by esterification [33]. Specifically, acetic acid rose markedly at F12 and then declined sharply at F24; this decline coincided with a significant increase in ethyl acetate at F24, consistent with acetic acid serving as its acyl donor [34]. Moreover, 2-octenoic acid, 3-methyldecanoic acid, and 2-ethylhexanoic acid showed a continuous post-fermentation

decrease, mainly because they participated in esterification, such that consumption exceeded formation and overall acid content fell.

3.4.5. Ketones

Ketones first increased and then decreased, peaking at F48, in line with previous findings [35]. The contents of 1-octen-3-one, 2-nonanone, (*E*, *E*)-3,5-octadien-2-one, 3-octanone, 2-decanone, and 2-tridecanone all increased significantly for the first time at F48, a hallmark of the transition from primary to secondary metabolism. This pattern is consistent with β-oxidation and the lipoxygenase (LOX)-type lipid oxidation pathway [36], as well as oxidation of 1-octen-3-ol to 1-octen-3-one. The later-stage ketone decrease may reflect their consumption by *Lp. plantarum* as alternative carbon sources.

3.4.6. Heterocyclic Compounds

Although heterocyclic compounds accounted for only a small proportion of the volatile flavor profile, they exerted a pronounced impact on flavor and typically impart caramel, nutty, floral, and fruity aroma characteristics. The 46 heterocyclic compounds identified in this study mainly comprised four major categories: furans, pyridines, pyrazines, and pyrroles. As shown in Figure 5a, the total heterocyclic content increased continuously after fermentation, with no significant difference between F72 and F96 at the later stage. As illustrated in Figure 5d–h, 2-ethyl-6-methylpyridine, 1-(5-methylpyrazin-2-yl) ethan-1-one, 5-ethylfuran-2-carbaldehyde, and dihydrofuran-2(5*H*)-one were significantly elevated after fermentation. With the exception of a minor contribution from the Maillard reaction during microwave sterilization, the post-fermentation increase in heterocyclic compounds was predominantly driven by Strecker degradation and other enzymatic conversions mediated by microbial metabolism [37]. During fermentation, microbially secreted extracellular proteases and glycosidases degraded proteins and polysaccharides into free amino acids and reducing sugars. The amino acids underwent Strecker degradation to generate aldehydes and nitrogen-containing heterocyclic precursors, which subsequently cyclized to form pyrazines, pyridines, and related compounds; concurrently, the reducing sugars underwent enzymatic dehydration and ring-closure to yield oxygen-containing heterocycles such as furfural and furanones. It should be noted that the pyrazine species resolved by GC-IMS (e.g., 2,3-dimethylpyrazine, noted in Section 3.3) are not identical to those quantified by GC×GC-TOFMS (e.g., 2-ethyl-6-methylpyrazine, Table 1); the two platforms differ in separation selectivity and detection sensitivity, and they therefore resolve overlapping but non-identical subsets of the pyrazine fraction.

Table 1. Compounds with *rOAV* ≥ 1 in at least one fermentation stage.

No	Volatile Compounds	Threshold (μg/kg)	*rOAV*						Odor
			UF	F12	F24	F48	F72	F96	
	Heterocyclic compounds								
1	2,5-Dimethyl-3-(3-methylbutyl)pyrazine	0.3	11.41 ± 0.2 ^{ab}	11.6 ± 0.81 ^{a}	10.34 ± 0.62 ^{bc}	9.49 ± 0.83 ^{c}	12.19 ± 0.84 ^{a}	7.89 ± 0.37 ^{d}	nutty, roasted, earthy, potato
2	4,5-Dimethyldihydrofuran-2(3H)-one	5	3.3 ± 0.14 ^{b}	3.27 ± 0.21 ^{b}	3.7 ± 0.10 ^{a}	2.67 ± 0.10 ^{c}	3.43 ± 0.31 ^{ab}	3.43 ± 0.09 ^{ab}	sweet, caramel, creamy, milky
3	3-Ethyl-2,5-dimethylpyrazine	5	1.64 ± 0.03 ^{a}	1.61 ± 0.10 ^{a}	1.04 ± 0.02 ^{b}	1.69 ± 0.16 ^{a}	1.49 ± 0.23 ^{a}	1.55 ± 0.04 ^{a}	nutty, roasted, burnt
4	2-Ethenyl-6-methylpyrazine	0.12	12.38 ± 0.38 ^{bc}	15.47 ± 1.15 ^{a}	11.78 ± 0.89 ^{bc}	11.78 ± 0.45 ^{bc}	12.88 ± 1.14 ^{b}	11.07 ± 0.73 ^{c}	roasted, smoky, herbaceous
5	2-Ethyl-6-methylpyrazine	0.15	N.D.	N.D.	N.D.	12.29 ± 1.99 ^{b}	9.47 ± 1.47 ^{c}	18.39 ± 1.69 ^{a}	roasted, nutty, meaty, malty
6	3,5-Diethyl-2-methylpyrazine	0.5	2.18 ± 0.15 ^{a}	1.85 ± 0.07 ^{c}	2.14 ± 0.19 ^{ab}	1.66 ± 0.09 ^{c}	1.89 ± 0.21 ^{bc}	1.69 ± 0.07 ^{c}	nutty, roasted, potato, vegetable

Table 1. *Cont.*

No	Volatile Compounds	Threshold (μg/kg)	*rOAV*						Odor
			UF	F12	F24	F48	F72	F96	
7	Rose Oxide	0.4	2.7 ± 0.5 ^{b}	3.74 ± 0.11 ^{a}	1.84 ± 0.50 ^{c}	2.14 ± 0.28 ^{bc}	1.82 ± 0.3 ^{c}	1.82 ± 0.09 ^{c}	rose, lemon, herbaceous
	Aldehydes								
8	2,4-Nonadienal	0.05	151.74 ± 12.77 ^{d}	214.64 ± 24.05 ^{c}	349.57 ± 52.91 ^{b}	393.69 ± 36.17 ^{b}	480.37 ± 36.05 ^{a}	145.46 ± 15.3 ^{d}	green, fatty, cucumber, melon
9	Octanal	0.7	10.04 ± 1.7 ^{b}	8.94 ± 1.11 ^{b}	5.35 ± 0.44 ^{c}	5.22 ± 0.56 ^{c}	14.24 ± 1.82 ^{a}	10.29 ± 1.44 ^{b}	lemon, citrus, green
10	(*E*)-2-Methyl-2-butenal	3.5	0.96 ± 0.01 ^{b}	0.96 ± 0.07 ^{b}	0.96 ± 0.01 ^{b}	0.97 ± 0.07 ^{b}	1.1 ± 0.12 ^{a}	0.89 ± 0.05 ^{b}	green, pungent, apple
11	(*E*)-2-Heptenal	4.2	0.5 ± 0.08 ^{d}	5.73 ± 0.64 ^{a}	5.54 ± 0.18 ^{a}	5.67 ± 0.03 ^{a}	4.48 ± 0.69 ^{b}	2.02 ± 0.14 ^{c}	green, fatty, almond, fresh
12	Undecanal	0.5	4.39 ± 0.18 ^{b}	2.17 ± 0.3 ^{c}	6.27 ± 1.70 ^{a}	2.7 ± 0.33 ^{c}	2.72 ± 0.57 ^{c}	2.6 ± 0.10 ^{c}	waxy, citrus, floral
13	2-Methylbutanal	1	0.87 ± 0.12 ^{c}	0.88 ± 0.08 ^{c}	1.22 ± 0.10 ^{ab}	1.37 ± 0.12 ^{a}	1 ± 0.18 ^{bc}	1.44 ± 0.19 ^{a}	cocoa, almond, nutty
14	Pentanal	12	2.36 ± 0.23 ^{cd}	1.48 ± 0.15 ^{d}	2.46 ± 0.40 ^{c}	5.62 ± 0.47 ^{a}	3.97 ± 0.69 ^{b}	4.49 ± 0.79 ^{b}	pungent, green, fruity, almond
	Esters								
15	Ethyl acetate	5	9.14 ± 0.52 ^{e}	27.14 ± 2.08 ^{c}	42.96 ± 5.44 ^{b}	24.86 ± 1.48 ^{c}	56.16 ± 2.08 ^{a}	17.51 ± 1.35 ^{d}	fruity, sweet, green
16	Ethyl (*E*)-9-octadecenoate	0.8	200.91 ± 7.1 ^{c}	202.35 ± 28.96 ^{c}	229.11 ± 20.18 ^{bc}	264.58 ± 29.08 ^{b}	321.84 ± 20.38 ^{a}	262.24 ± 30.99 ^{b}	waxy, fatty, milky
17	Ethyl octanoate	2	5.55 ± 0.71 ^{c}	6.26 ± 0.3 ^{c}	8.34 ± 0.81 ^{c}	19.25 ± 2.77 ^{a}	13.01 ± 1.78 ^{b}	15.09 ± 1.3 ^{b}	fruity, sweet
18	Geranyl formate	10	1.54 ± 0.09 ^{a}	1.53 ± 0.06 ^{a}	1.34 ± 0.09 ^{bc}	1.46 ± 0.09 ^{ab}	1.22 ± 0.1 ^{c}	1.32 ± 0.04 ^{bc}	rose, lemon, fruity
	Ketones								
19	(*E*, *E*)-3,5-Octadien-2-one	0.8	2.28 ± 0.16 ^{c}	2.72 ± 0.04 ^{b}	2.3 ± 0.3 ^{c}	4.18 ± 0.21 ^{a}	2.76 ± 0.35 ^{b}	2.61 ± 0.05 ^{bc}	pungent, green, fruity, floral
20	1-Octen-3-one	0.01	1459.75 ± 222.49 ^{b}	1420.77 ± 200.99 ^{b}	1622.85 ± 149.15 ^{b}	1883.86 ± 185.65 ^{a}	1303.3 ± 106.03 ^{bc}	1026.55 ± 108.04 ^{c}	mushroom, green
21	2,3-Octanedione	5	5.31 ± 0.78 ^{b}	2.34 ± 0.1 ^{d}	4.95 ± 0.24 ^{b}	6.13 ± 0.13 ^{a}	2.81 ± 0.11 ^{cd}	3.25 ± 0.6 ^{c}	creamy, buttery, sweet
22	6-Methyl-3,5-heptadien-2-one	3	2.31 ± 0.08 ^{c}	3.12 ± 0.23 ^{a}	2.6 ± 0.06 ^{bc}	2.9 ± 0.14 ^{ab}	3.19 ± 0.27 ^{a}	2.72 ± 0.18 ^{b}	green, pungent, fruity
	Acids								
23	2,3-Dimethylpentanoic acid	2	1.26 ± 0.01 ^{a}	1.26 ± 0.15 ^{a}	1.45 ± 0.03 ^{a}	1.41 ± 0.05 ^{a}	1.39 ± 0.23 ^{a}	0.94 ± 0.04 ^{b}	cheesy, sweaty, fatty
	Alkenes								
24	β-Myrcene	15	0.77 ± 0.05 ^{d}	1.4 ± 0.03 ^{a}	1.02 ± 0.01 ^{c}	1.05 ± 0.01 ^{bc}	1.04 ± 0.03 ^{bc}	1.09 ± 0.04 ^{b}	geranium, spicy, peppery, musty

Different lowercase letters within a row indicate significant differences among fermentation stages according to the statistical methods described in Section 2.6 ($p < 0.05$). Odor thresholds were taken from van Gemert [21], using values reported in water. N.D., Not detected.

3.4.7. Others

The overall content of aromatic hydrocarbons peaked at F48, following a trend similar to that of ketones. This pattern is likely attributed to their consumption as carbon sources by microorganisms during the late stage of fermentation. Previous studies have reported similar phenomena, confirming that this is related to the microbial degradation of aromatic compounds [38]. Notably, among the alkenes, except for the F12 group, which had a higher content than the UF, all other fermented groups showed lower levels than UF and exhibited a continuous downward trend. Microbial biotransformation can convert certain alkenes or alkene-derived precursors into alcohols, aldehydes, ketones, and esters, thereby contributing to the formation of VFCs [39]. The alkene compounds most abundant in UF, including cyclooctatetraene, longifolene, and γ-muurolene, underwent varying degrees of reduction. α-Dehydro-ar-himachalene was significantly enriched at F24, originating from microbial transformation of plant terpenoid precursors and contributing woody and herbal notes [40]. In contrast to the decline in alkenes, the content of phenols increased continuously, which is mainly attributed to the microbial hydrolysis and gradual release of endogenous macromolecular polyphenols from the SLSP. As fermentation proceeds, the cell wall structure of the SLSP is degraded, thereby facilitating the release of these polyphenols [8].

Collectively, *Lp. plantarum* fermentation drastically remodeled flavor-related metabolic networks in SLSP, reshaping the volatile flavor profile. At the F72 time point, the total content of VFCs reached its maximum, exhibiting an ester-dominated aroma profile. Meanwhile, the contents of aldehydes and heterocyclic compounds ceased to increase, indicating that 72 h of fermentation represents the critical period for flavor development.

3.5. rOAV Analysis

The overall aroma profile of a food matrix is determined not only by the concentration and odor quality of individual volatiles but also critically by their odor thresholds. The *rOAV*, defined as the ratio of the concentration of an individual volatile compound to its odor threshold in a given matrix, was used to identify the VFCs that actively contribute to the aroma of SLSP at each fermentation stage. Compounds with $rOAV \geq 1$ are generally considered odor-active [41]. Because the odor thresholds were compiled in water, the *rOAV*s were interpreted as relative rather than absolute indicators of odor contribution in this matrix. Among the 264 VFCs quantified, 24 exhibited $rOAV \geq 1$ in at least one fermentation stage, including 7 heterocyclics, 7 aldehydes, 4 ketones, 4 esters, 1 acid, and 1 alkene.

1-Octen-3-one emerged as the most dominant aroma contributor throughout the fermentation process, exhibiting *rOAV* values ranging from 1026.6 ± 108.0 (F96) to 1883.9 ± 185.7 (F48) (Table 1). Its *rOAV* was consistently 3- to 7-fold higher than that of the second-ranked odorant at each stage (typically 2,4-nonadienal; *rOAV* 145.5–480.4; green, fatty, cucumber-like), confirming that the characteristic mushroom note serves as the signature aroma of SLSP. Ethyl (*E*)-9-octadecenoate (*rOAV* 200.9–321.8; waxy, fatty, milky) and ethyl acetate (*rOAV* 9.1–56.2; fruity, sweet) acted as secondary contributors, with the latter reaching its peak at F72. Although certain pyrazines exhibited moderate *rOAV*s (e.g., 2-ethyl-6-methylpyrazine up to 18.4 at F96; 2-ethenyl-6-methylpyrazine up to 15.5 at F12), their absolute values remained substantially lower than those of 1-octen-3-one, indicating that roasted/nutty notes play a supplementary rather than a dominant role.

The overall aroma intensity, as reflected by both the number of odor-active compounds and the magnitude of their *rOAV*s, peaked at F72: all 24 selected compounds exhibited $rOAV \geq 1$ at this stage, compared to only 19 at the UF. At F72, 2,4-nonadienal (480.4 ± 36.1), ethyl acetate (56.2 ± 2.1), and ethyl (*E*)-9-octadecenoate (321.8 ± 20.4) simultaneously reached their maximum *rOAV*s. However, a distinct stylistic shift occurred from F72 to F96: the mushroom-associated 1-octen-3-one decreased by approximately 21% (from 1303.3 to 1026.6), and the green/fatty 2,4-nonadienal dropped sharply to 145.5 ± 15.3, whereas roasted/meaty pyrazines continued to increase. Specifically, 2-ethyl-6-methylpyrazine, which was not detected prior to F48, rose to its highest *rOAV* (18.4 ± 1.7) at F96. Concurrently, the number of compounds with $rOAV \geq 1$ decreased to 22.

In terms of chemical classes, ketones dominated the *rOAV* profile exclusively due to 1-octen-3-one. Aldehydes contributed primarily through 2,4-nonadienal and, to a lesser extent, octanal and (*E*)-2-heptenal; esters contributed via ethyl (*E*)-9-octadecenoate and ethyl acetate. Although the heterocyclic subclass was low in total abundance, it exerted a growing sensory impact during the later fermentation stages, driven by pyrazines and furanones (e.g., 4,5-dimethyldihydrofuran-2(3*H*)-one, *rOAV* 2.7–3.7; sweet, caramel-like) [42]. Within the pyrazine subgroup, the trajectories were heterogeneous: 2,5-dimethyl-3-(3-methylbutyl) pyrazine decreased at F96 (from 12.2 to 7.9), whereas 2-ethyl-6-methylpyrazine and 2-ethenyl-6-methylpyrazine remained high or increased. This indicates that the roasted/meaty impression at F96 is driven by specific pyrazines rather than the pyrazine class as a whole. Acids contributed only marginally, represented solely by 2,3-dimethylpentanoic acid (*rOAV* 0.94–1.45; cheesy, sweaty). Alkenes were represented by β-myrcene, whose *rOAV* remained

near or below unity (0.77–1.4), indicating a negligible direct sensory contribution despite its relatively high abundance.

In summary, *rOAV* analysis revealed that fermentation progressively restructured the aroma of SLSP from a simple mushroom-dominated profile in UF into a balanced, multi-note system at F72, in which the mushroom anchor (1-octen-3-one), green/fatty character (2,4-nonadienal), and fruity/waxy esters (ethyl acetate, ethyl (*E*)-9-octadecenoate) simultaneously reached their maxima and all 24 odor-active compounds exceeded their thresholds. However, extending fermentation to F96 did not further enrich the desirable aroma but instead led to its deterioration: the signature mushroom odorant decreased by 21%, the green/fatty 2,4-nonadienal dropped to less than one-third of its F72 value, and the total number of odor-active compounds declined from 24 to 22. The modest increase in pyrazines at F96, with a maximum *rOAV* of approximately 18.4, was insufficient to compensate for these losses. Consequently, the F96 profile exhibited reduced odor-active content, characterized by a weakened mushroom core, attenuated fruity and green notes, and an emerging but unbalanced roasted and sulfury undertone; extending fermentation to 96 h did not further increase the content of odor-active volatiles. This *rOAV*-based deterioration independently supports F72 as the endpoint of aroma-active accumulation, beyond which prolonging fermentation does not yield additional gains in odor-active content.

It should be noted that the odor descriptors assigned to individual VFCs in this section (e.g., mushroom, green, fatty, fruity) are taken from the published literature rather than from direct GC-olfactometry or trained sensory-panel evaluation performed in this study. The *rOAV*-based ranking therefore indicates which volatiles are likely to contribute to the aroma profile, but the actual perceived odor quality and intensity of SLSP at each stage remain to be confirmed by a trained sensory panel in future work.

3.6. LC-MS Analysis

Non-targeted LC-MS detected a total of 334 metabolites. These compounds were annotated by multi-library MS/MS spectral matching, with confirmation based on m/z error < 5 ppm, molecular formula, and adduct ion validation. The identified metabolites were assigned to MSI Level 1 ($n = 53$), Level 2 ($n = 253$), and Level 3 ($n = 28$) (Table S2). OPLS-DA was applied to the six fermentation groups, yielding $R^2X(cum) = 0.896$, $R^2Y(cum) = 0.991$, and $Q^2(cum) = 0.803$, indicating good model fit and predictive ability. Model reliability was further confirmed by a 200-permutation test (R^2 intercept = 0.706, Q^2 intercept = −0.578) and CV-ANOVA ($p < 0.001$, F = 4.27); the negative Q^2 intercept and the significant CV-ANOVA *p*-value together demonstrate that the model was not overfitted and the group discrimination was not driven by random chance.

As shown in the OPLS-DA score scatter plot (Figure 6a), the UF was clearly separated from the five fermentation-time groups along the t[1] axis: UF samples were located in the positive region, whereas all fermented samples were distributed in the negative region, indicating that fermentation induced a pronounced overall remodeling of the metabolome. Meanwhile, the fermented samples exhibited a clear time-dependent gradient along the t[2] axis: the early-stage groups F12 and F24 lay in the upper region, the intermediate F48 in the middle, and the late-stage groups F72 and F96 in the lower region. This gradient demonstrated that fermentation time was the key factor driving metabolomic differentiation and that the metabolite profile evolved continuously throughout fermentation. The three biological replicates within each group clustered tightly, further confirming the reproducibility of the LC-MS data and the stability of the model.

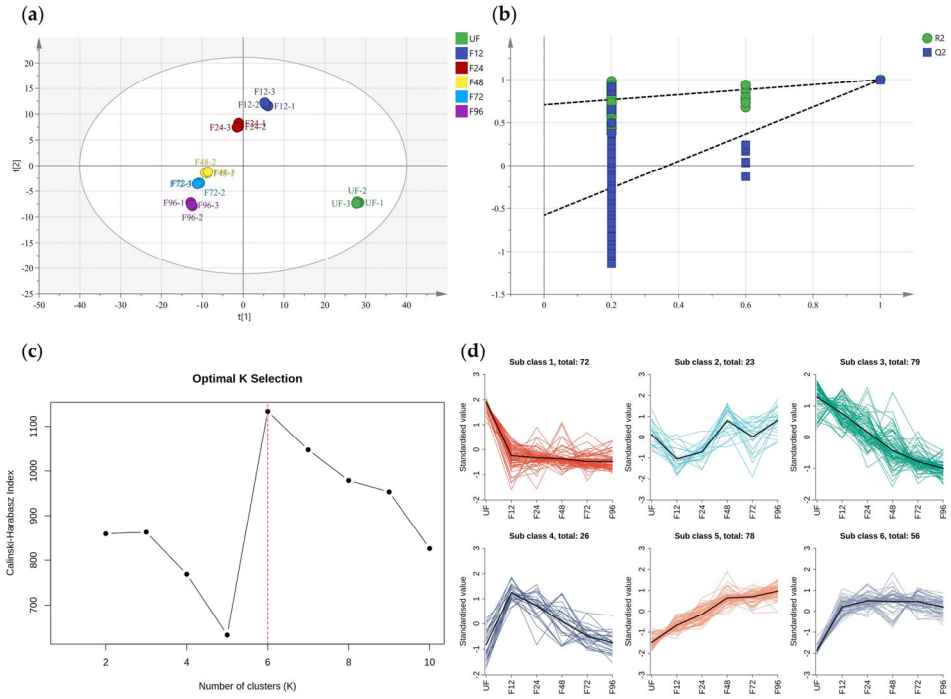


Figure 6. Multivariate and clustering analysis of the non-volatile metabolome of SLSP during fermentation with *Lp. plantarum*. (**a**) OPLS-DA score plot. (**b**) 200-permutation test. (**c**) Calinski-Harabasz index for determination of the optimal number of clusters. (**d**) k-means clustering of metabolite temporal profiles into six subclusters.

To characterize temporal variation patterns, k-means clustering was performed on the features based on their standardized profiles across the six time points (UF, F12, F24, F48, F72, and F96). As shown in Figure 6c, the Calinski–Harabasz (CH) index (Section 2.6) reached its maximum at k = 6, and therefore k = 6 was selected. As shown in Figure 6d, the six subclusters (C1–C6) covered all 334 metabolites, with sizes of C1 = 72, C2 = 23, C3 = 79, C4 = 26, C5 = 78, and C6 = 56. Compounds in C1 displayed a dilution or baseline-maintenance pattern, with all 72 metabolites reaching their maximum at UF and the median abundance falling to 0.32-fold and 0.30-fold the UF level at F72 and F96, respectively. This cluster comprised mainly the endogenous primary metabolites of SLSP that were inherently abundant in the starting material, including free amino acids (*trans*-4-hydroxyproline, aspartate, glutamine, citrulline), TCA and related organic acids (citric acid, malic acid, gluconic acid), soluble sugars and polyols (*D*-xylose, *D*-fucose, volemitol, arabinitol), and endogenous fatty acids and their basal oxidation products (palmitelaidic acid, linolenic acid, azelaic acid). These metabolites were progressively diluted or slowly utilized upon fermentation but were not substantially newly synthesized. C1 therefore represents the native background metabolome against which fermentation-induced changes in the other clusters are measured; the presence of oxylipins already at UF further indicates that a low baseline of lipid oxidation existed in the starting dry powder prior to fermentation.

C2 was a small transitional cluster of 23 metabolites whose abundance remained largely stable across fermentation, with individual peaks distributed at F48 (10 metabolites) and F96 (9 metabolites). Members included phenylacetaldehyde, methionine, acetyl-CoA, 9-HPODE, α-*D*-glucose, *N*-acetyl-*D*-hexosamine, and several small peptides (Pro-Ala, Lys-Val, Pro-Hyp). Their near-constant abundance suggests a steady-state balance between microbial formation and further turnover rather than a directional accumulation or depletion, and this cluster contributed little to the F72 endpoint signature.

C3 exhibited a continuous-consumption pattern, with 57 of 79 metabolites reaching their maximum at UF and 17 additional metabolites peaking transiently at F12; the median abundance declined progressively to 0.54-fold and 0.46-fold the UF level at F72 and F96. This cluster was dominated by free amino acids and derivatives (tryptophan, histidine, proline, *N*-methylleucine, 3-methoxytyramine), long-chain fatty acids and sphingoid bases (myristic acid, behenic acid, γ-linolenic acid, C17-sphingosine, hexadecasphingosine), central metabolic intermediates (α-ketoglutarate, aconitic acid, ascorbic acid, pantothenic acid, thioctic acid), and phosphorylated or storage sugars (glucosamine, sorbitol 6-phosphate, trehalose 6-phosphate, fructofuranose 6-phosphate) together with purine derivatives (xanthosine, inosine). This persistent consumption of the native amino-acid, fatty-acid, and carbohydrate pools was temporally reciprocal with the accumulating C5 peptide and C6 LAB-product clusters, consistent with substrate-to-product conversion in which endogenous macromolecules were degraded and reassembled into shorter peptides during fermentation.

C4 reflected a transient early-stage response, with 18 of 26 metabolites peaking at F12 (median 1.5-fold relative to UF) and returning to below-UF levels by F72. This cluster included tryptamine, N^8-acetylspermidine, *N*-acetylthreonine, lysylproline, sebacic acid, itaconic acid, glycerol 2-phosphate, fructose, succinic acid, and threonyllysine. Their short-lived rise immediately after inoculation is consistent with an adaptive microbial response to the new substrate, characterized by polyamine synthesis, initial TCA engagement, and rapid monosaccharide consumption. This pattern suggests that these compounds do not primarily shape the final flavor. The response was largely resolved by mid-fermentation and contributed minimally to the F72 endpoint.

C6 represented the mid-fermentation product pool, with median abundance rising sharply to 5.2-fold the UF level at F24 and remaining elevated through F48 (5.1-fold), F72 (4.5-fold), and F96 (4.1-fold). This cluster was dominated by two flavor-relevant subgroups. The first consisted of LAB-derived acidic metabolites, including indole-3-lactic acid, (*R*)-3-phenyllactic acid, *L*-leucic acid, and pelargonic acid, which are consistent with amino-acid catabolism and fatty-acid hydroxylation by *Lp. plantarum*. The second subgroup comprised lipid-related metabolites, including avenoleic acid, linoleamide, 12-HHTrE, (9*E*)-12-hydroxyoctadec-9-enoic acid, (*R*)-2-hydroxystearic acid, 2-hydroxyoctadecanoic acid, 17-octadecynoic acid, and elaidic acid, alongside a set of medium peptides (Phe-Gln, Lys-Leu, Tyr-Gln, His-Gln, His-Tyr, Tyr-Leu, Pro-Ile, Lys-Gln, Leu-Leu-Leu). These lipid-related members rose early (F12–F24), plateaued around F24–F72, and softened only modestly by F96, consistent with a precursor-to-product pattern linking endogenous lipid turnover to downstream volatile aldehydes, alcohols, and esters.

C5 showed the most pronounced continuous-accumulation pattern, with median abundance rising progressively from 2.9-fold the UF level at F12 to 14.0-fold at F96, and 57 of 78 metabolites reaching their maximum at F96 (an additional 13 and 8 peaked at F48 and F72, respectively). This cluster was dominated by di- and tripeptides (e.g., Phe-Val-Lys, Glu-Arg, Val-Val, cyclo(Phe-Leu), Phe-Phe, Ile-Leu, Val-Leu, Phe-Glu, Tyr-Ile-Asp, Tyr-Ile-Asn, Ala-Gly-Arg, Ile-Val-Glu, β-Ala-Arg, Ile-Lys-Glu, Leu-Leu-Leu), together with indole derivatives (indole-3-acetic acid ethyl ester, indoleacetic acid, tryptoline) and a small number of other microbial metabolites (jasmonoyl-isoleucine, lumichrome, homophenylalanine). These results indicate that, after 48 h, microbial peptidases progressively hydrolyzed the substrate's macromolecular proteins, continuously releasing short peptides that accumulated during the later stages and constituted a major source of umami taste and potential bioactive peptides. Because the vast majority of these peptides are non-volatile, their continued accumulation beyond 72 h contributes to taste rather than to aroma. Overall, the six clusters delineate two asynchronous trajectories after F72. The C6 lipid-related and acidic LAB precursors attained their maximum around F24–F72 (median 4.5-fold at F72, with most

members already at or near their peak) and softened only modestly by F96 (median 4.1-fold). Meanwhile, the C1 background metabolome and the C3 pool of free amino acids, long-chain fatty acids, and phosphorylated sugars were already largely exhausted at this stage, and the transient C4 response had long since resolved, while the small C2 transitional pool remained essentially flat. By contrast, the taste layer, represented by C5 di- and tripeptides, continued to rise between F72 and F96 (median 14.0-fold at F96 versus 12.9-fold at F72). However, these peptides are non-volatile and therefore contribute only to umami taste, not to the aroma. This divergence indicates that aroma-relevant precursor accumulation had essentially plateaued by 72 h, while taste-active peptide accumulation persisted. In agreement with the volatile data (Sections 3.4 and 3.5), total VFC content was maximal at F72 and declined at F96, and all 24 odor-active volatiles exceeded their thresholds at F72. Extending fermentation to 96 h therefore enriched the non-volatile peptide fraction while failing to further improve and actually weakening the volatile aroma. F72 thus represents the point at which aroma-relevant precursor accumulation and odor-active volatile content reach their maximum, coinciding with the near-depletion of the native amino-acid and lipid pools. This provides a metabolically justified cutoff rather than an empirically set time point.

3.7. E-Tongue Analysis of the Taste Profile

The taste profiles of SLSP at the six fermentation stages were further evaluated by E-tongue. As illustrated in Figure 7a, the PCA model exhibited clear separation, with PC1 and PC2 together accounting for over 90% of the total variance, and the model yielded $R^2X(cum) = 0.993$ and $Q^2(cum) = 0.969$. This indicates that the E-tongue is an effective tool for swiftly distinguishing between SLSP prior to and following fermentation with *Lp. plantarum*.

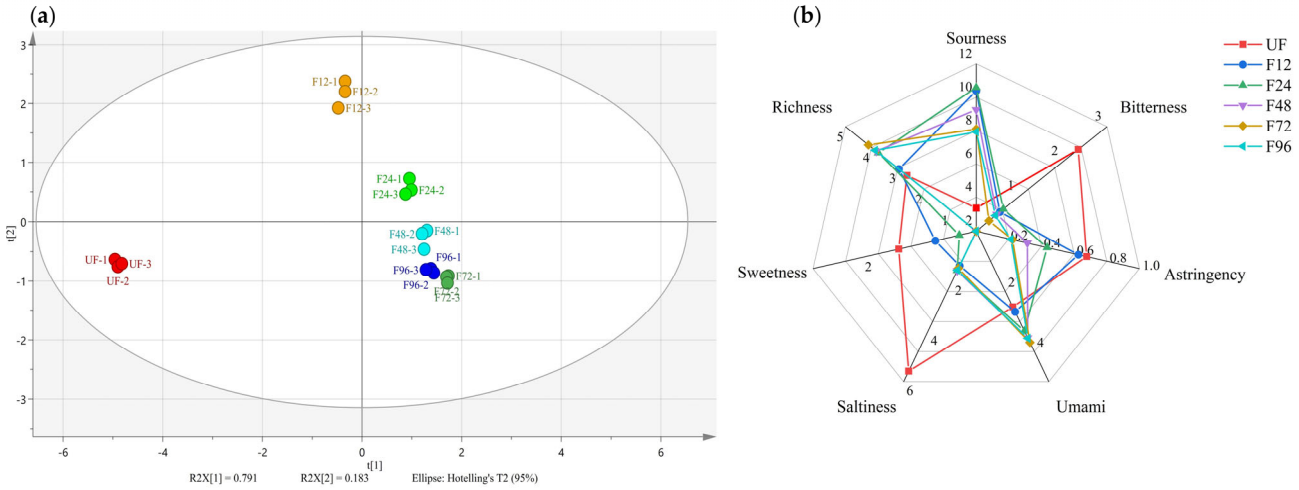


Figure 7. E-tongue taste profile of *Lp. plantarum*-fermented SLSP across the six fermentation stages (UF, F12, F24, F48, F72, and F96). (**a**) E-tongue PCA plot; (**b**) E-tongue radar chart.

The radar plot (Figure 7b) illustrates the response patterns of UF and F12–F96 across the seven taste dimensions. The results indicate that fermentation significantly reshaped the overall taste profile of SLSP. Sourness increased sharply at F24 and reached its highest level at this stage. Then it gradually decreased with prolonged fermentation, yet remained markedly higher than in UF throughout the process. This trend reflects the rapid acid production by *Lp. plantarum* during early fermentation, which aligns well with the accumulation of lactic acid and serves as a key factor driving flavor transformation [43]. Umami and richness both exhibited an initial increase followed by stabilization, entering a plateau

phase during F72–F96. This suggests that intensified proteolysis during fermentation facilitated the liberation of free amino acids and savory oligopeptides, jointly elevating the umami intensity and sensory complexity of SLSP [44]. Furthermore, compared with UF, the values for astringency, bitterness, and saltiness decreased significantly in the F12–F96 samples, indicating that fermentation effectively improved the taste of SLSP. Sweetness decreased rapidly and maintained an extremely low response value from F48 onwards. This observation is attributed to the utilization of sugars as a carbon source by *Lp. plantarum*, which consumed substantial amounts of carbohydrates to produce organic acids such as lactic acid and acetic acid, thereby explaining the concurrent rapid increase in sourness [45].

Collectively, the E-tongue results demonstrated that extending fermentation beyond 72 h conferred no additional taste benefit, whereas the volatile analysis (Sections 3.2–3.5) showed that the total content of odor-active volatiles declined after 72 h. The absence of further taste development at 96 h therefore reinforces 72 h as the endpoint of aroma-active metabolite accumulation, in agreement with the physiological and volatile-flux evidence described above.

3.8. Correlation Analysis Between VFCs and Non-Volatile Precursor Metabolites

To establish quantitative links among the non-volatile precursor pool, the volatile aroma compounds, and the perceived gustatory attributes, Spearman rank correlation analysis was performed across the three analytical layers using $\log_2(x + 1)$-transformed data from 18 individual samples (6 stages × 3 biological replicates).

The variable set comprised (i) the 24 volatile compounds with $rOAV \geq 1$ (Table 1), considered odor-active; (ii) 27 representative non-volatile metabolites selected from the six k-means subclusters to capture the full spectrum of precursor dynamics; and (iii) the seven E-tongue taste dimensions. The 27 non-volatile metabolites included C6 lipid-derived aroma precursors and LAB-derived acids (linoleamide, elaidic acid, 17-octadecynoic acid, (9*E*)-12-hydroxyoctadec-9-enoic acid, (*R*)-2-hydroxystearic acid, 2-hydroxyoctadecanoic acid, sebacic acid, (*R*)-3-phenyllactic acid, indole-3-lactic acid), C5 taste-active di- and tripeptides and signaling molecules (Tyr-Ile-Asp, Leu-Leu-Leu, Val-Leu, Arg-Trp-Ile, Ile-Val-Glu, (−)-jasmonoyl-L-isoleucine), C1/C3 depleted substrate pools (γ-linolenic acid, linolenic acid, 9-oxoODE, citric acid, *L*-malic acid, *L*-tryptophan, *L*-proline, glutamine), and C4 transient-response markers (12,13-dihydroxy-9-octadecenoic acid, tryptamine, succinic acid, N^8-acetylspermidine). This three-layer design tests whether the temporal accumulation of non-volatile precursors statistically tracks the formation of specific aroma compounds and the intensification of corresponding taste attributes. Correlations with $|\rho| > 0.7$ and Benjamini–Hochberg FDR-adjusted $p < 0.05$ were considered significant (Figure 8).

A total of 98 significant correlation pairs were identified (55 positive, 43 negative). The C1/C3 depleted substrate pool showed the highest number of correlations (34 pairs, dominated by negative correlations), followed by C5 peptides (28), C6 lipid-derived precursors and LAB acids (26), and C4 transient markers (10). Volatile–precursor associations. The formation of ethyl esters was closely coupled with C6 lipid-derived precursors and LAB acids: ethyl acetate was positively correlated with elaidic acid ($\rho = 0.744$), 2-hydroxyoctadecanoic acid ($\rho = 0.728$), and sebacic acid ($\rho = 0.734$), while ethyl (*E*)-9-octadecenoate was positively correlated with indole-3-lactic acid ($\rho = 0.847$), (*R*)-3-phenyllactic acid ($\rho = 0.833$), 12,13-dihydroxy-9-octadecenoic acid ($\rho = 0.725$), and N^8-acetylspermidine ($\rho = 0.754$). Ethyl octanoate was positively correlated with Tyr-Ile-Asp ($\rho = 0.748$), Val-Leu ($\rho = 0.818$), and Ile-Val-Glu ($\rho = 0.808$), indicating that ester accumulation tracked both lipid-derived precursors and short-peptide dynamics. In contrast, γ-linolenic acid displayed strong negative correlations with ethyl octanoate ($\rho = -0.868$), 2-methylbutanal ($\rho = -0.808$), and pentanal ($\rho = -0.732$), consistent with its role as a consumed substrate for lipid-derived

volatile biosynthesis. (*E*)-2-Heptenal was positively correlated with 12,13-dihydroxy-9-octadecenoic acid (ρ = 0.825), N^8-acetylspermidine (ρ = 0.822), indole-3-lactic acid (ρ = 0.792), and (*R*)-3-phenyllactic acid (ρ = 0.736), and negatively with linolenic acid (ρ = −0.767), indicating that the accumulation of this aldehyde was temporally coupled with early membrane-turnover products rather than with the native substrate pool itself.

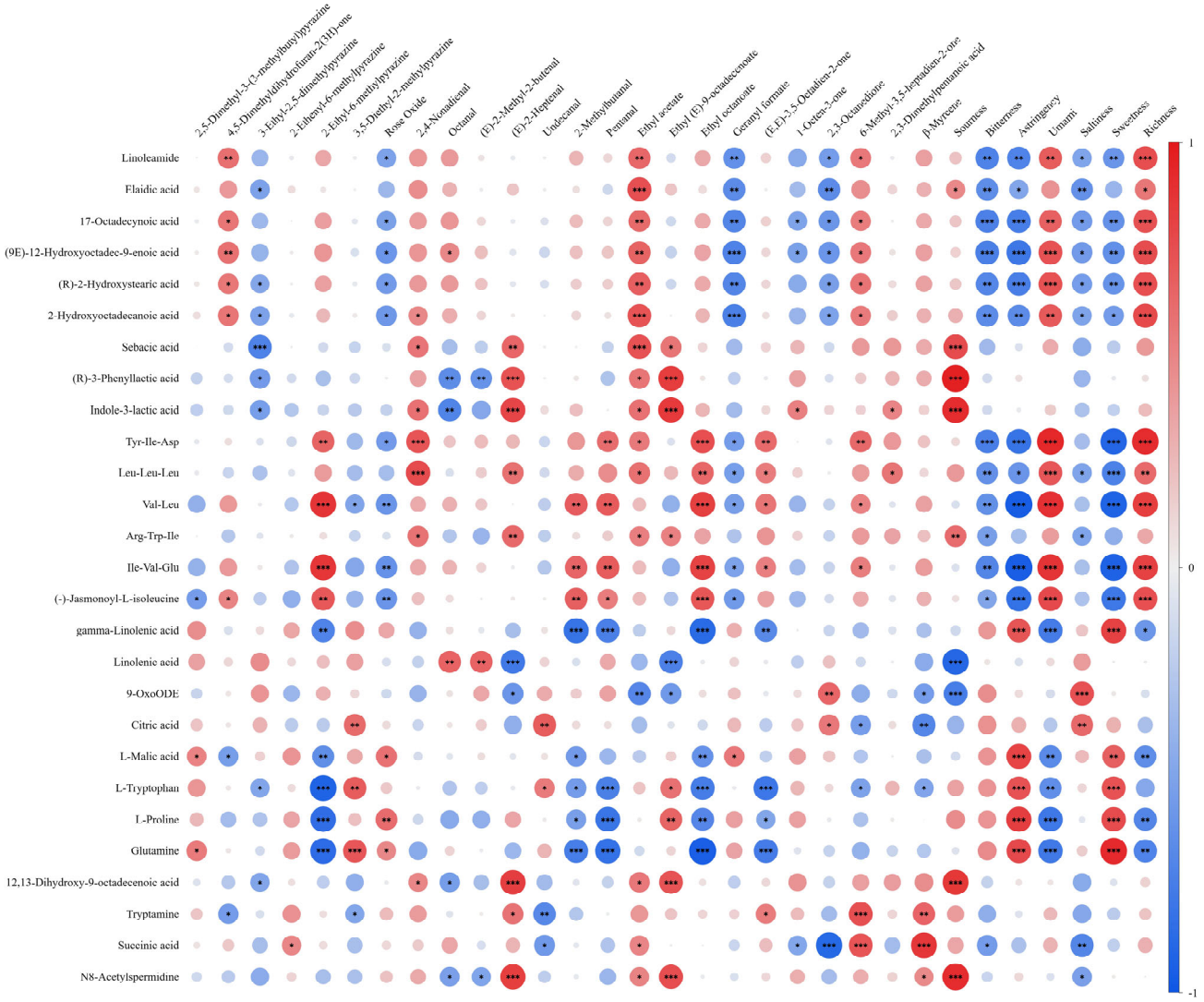


Figure 8. Spearman correlation heatmap among 24 odor-active volatiles (*rOAV* ≥ 1), 7 E-tongue taste dimensions, and 27 representative non-volatile metabolites from the six k-means subclusters across six fermentation stages of SLSP (UF, F12, F24, F48, F72, and F96). Red represents positive correlation, while blue represents negative correlation. A darker colour and larger circle area indicate a stronger correlation. *, ** and *** correspond to significance levels of $p < 0.05$, $p < 0.01$ and $p < 0.001$, respectively.

Umami output was most strongly and positively correlated with the tripeptide Tyr-Ile-Asp (ρ = 0.935) and the dipeptides Val-Leu (ρ = 0.891) and Ile-Val-Glu (ρ = 0.877), together with (−)-jasmonoyl-L-isoleucine (ρ = 0.777). Among established tastants, glutamine (ρ = −0.771) and L-proline (ρ = −0.777) declined as umami rose, consistent with substrate-to-product conversion. Richness output showed a parallel pattern, correlating positively with Tyr-Ile-Asp (ρ = 0.913), Val-Leu (ρ = 0.822), Ile-Val-Glu (ρ = 0.815), and the C6 lipid precursors 2-hydroxyoctadecanoic acid (ρ = 0.774), (9*E*)-12-hydroxyoctadec-9-enoic

acid ($\rho = 0.760$), linoleamide ($\rho = 0.757$), (*R*)-2-hydroxystearic acid ($\rho = 0.749$), and 17-octadecynoic acid ($\rho = 0.731$).

Sweetness output was positively associated with the native background metabolites glutamine ($\rho = 0.918$), γ-linolenic acid ($\rho = 0.815$), *L*-proline ($\rho = 0.766$), and *L*-tryptophan ($\rho = 0.735$), which were progressively consumed during fermentation. Of these, the native amino acids and residual sugar/polyol pool are plausible contributors to the initial sweet taste of raw SLSP, whereas γ-linolenic acid is itself sweet-tasting at elevated concentrations and serves here as a proxy for the undepleted native lipid pool. Sweetness was negatively correlated with Ile-Val-Glu ($\rho = -0.925$), Val-Leu ($\rho = -0.914$), Tyr-Ile-Asp ($\rho = -0.899$), and (−)-jasmonoyl-L-isoleucine ($\rho = -0.775$), reflecting the reciprocal relationship between native substrate depletion and peptide-driven taste maturation.

Sourness output was dominated by the LAB-derived acids (*R*)-3-phenyllactic acid ($\rho = 0.963$), indole-3-lactic acid ($\rho = 0.915$), and sebacic acid ($\rho = 0.763$), together with N^8-acetylspermidine ($\rho = 0.915$) and 12,13-dihydroxy-9-octadecenoic acid ($\rho = 0.860$). These are genuine sour-active compounds (phenyllactic acid and indole-lactic acid are established organic-acid tastants), and their strong coupling to sourness output is consistent with well-known acidification by *Lp. plantarum*. Sourness was negatively correlated with linolenic acid ($\rho = -0.893$) and 9-oxoODE ($\rho = -0.740$), the native lipid pool that was progressively oxidized as acidification proceeded. Bitterness and astringency outputs were negatively associated with several C6 lipid precursors (linoleamide, 17-octadecynoic acid, (9*E*)-12-hydroxyoctadec-9-enoic acid) and C5 peptides (Tyr-Ile-Asp, Val-Leu, Ile-Val-Glu, (−)-jasmonoyl-L-isoleucine), indicating that the accumulation of lipid-derived and peptide metabolites during fermentation was associated with a reduction in unpleasant taste output; mechanistically, this is more likely due to masking or pH/ionic-strength shifts detected by the sensors than to a direct bitter-masking action of these peptides.

Relationship between electronic sensors and sensory perception, and provenance of flavor compounds. The electronic tongue and electronic nose used in this study are rapid, non-targeted screening instruments rather than substitutes for human sensory panels. These metrics reflect the overall polarity, acidity, and volatile-profile similarity of the extracts; while they correlate with perceived taste and aroma intensity, they do not serve as direct measures of these sensory attributes. The correlations above should therefore be read as a metabolic timeline anchored to sensor output, not as a definitive receptor-level taste map. With respect to provenance, the C1/C3 pool (citric acid, malic acid, glutamine, proline, tryptophan, linolenic acid, γ-linolenic acid, native sugars and polyols) is largely substrate-derived, reflecting the native metabolome of raw S. latifolia powder; the C6 pool of hydroxy fatty acids, linoleamide, phenyllactic acid, and indole-3-lactic acid, together with the C5 short peptides, is fermentation-derived, generated by *Lp. plantarum* amino-acid catabolism, lipid hydroxylation, and extracellular proteolysis. This substrate-versus-fermentation dichotomy is consistent with previous reports on *Lp. plantarum* fermentation of plant and fungal matrices. Phenyllactic acid and indole-3-lactic acid are well-established LAB metabolites that accumulate during *Lp. plantarum* fermentation of mixed vegetables, where they were identified as signature organic acids by GC-TOF metabolomics [46], and their biosynthetic origin from phenylalanine and tryptophan catabolism has been reviewed recently [47]. Short-peptide accumulation with concomitant free-amino-acid depletion mirrors the proteolytic pattern described in *Lp. plantarum*-fermented shiitake mushrooms, where umami-associated glutamate, aspartate, and 5′-nucleotides increased over fermentation [48], and in fermented fruiting bodies of button, oyster, and shiitake mushrooms, where starter-culture *Lp. plantarum* degraded native protein and enriched polyunsaturated fatty acids [49]. The electronic-sensor approach used here is consistent with a recent review concluding that potentiometric e-tongue and e-nose outputs correlate significantly with

trained-panel sensory profiles but are best regarded as rapid screening proxies rather than substitutes for human evaluation [50].

Reported fermentation durations for *Lp. plantarum*-processed mushroom matrices include 48 h for a four-strain LAB consortium containing *Lp. plantarum* on button mushroom [51], 96 h for *Lp. plantarum* GDM1.191 on shiitake [48], and 120 h for *Lp. plantarum* on *Pleurotus eryngii* [10]. The 72 h endpoint determined in this study lies within this reported range and is consistent with our flavor-optimization goal, characterized by the peak accumulation of aroma-active metabolites at 72 h prior to the emergence of sulfur- and roast-derived off-notes at 96 h. Crucially, whereas those studies fixed the duration a priori, the endpoint here was defined by the convergence of volatile, non-volatile, and taste data, with the kinetic and physicochemical data confirming that substrate depletion and growth cessation had already occurred before 72 h. Although the optimal 72 h duration is specific to this substrate and strain, the proposed framework offers a transferable approach for defining endpoints in mushroom fermentations. Together, these correlation patterns indicate that the temporal accumulation of C6 lipid-derived and peptide metabolites was coupled with the formation of fruity and floral esters and with the intensification of umami and richness output and inversely associated with sweetness, bitterness, and astringency. These findings provide a correlative molecular framework for the flavor changes observed at the 72 h fermentation endpoint, with the caveat that electronic-sensor output is a proxy for, not a direct measure of, human sensory perception. This study has several limitations. The hydroxy-fatty acids and jasmonates central to the correlation network are mainly MSI Level 2 annotations, and their many isomeric forms cannot be fully resolved by LC-MS/MS spectral matching alone. Thus, individual precursor assignments should be interpreted cautiously, and the resulting correlation network is hypothesis-generating rather than confirmatory, even though the overall temporal coupling pattern remains robust across independent platforms. These caveats do not alter the principal finding that 72 h marks the peak of aroma-active accumulation and the plateau of taste development.

4. Conclusions

In this study, a multi-platform strategy integrating fermentation kinetics, E-nose, GC-IMS, GC×GC-TOFMS, non-targeted LC-MS, and E-tongue was used to define the fermentation endpoint of *Lp. plantarum*-fermented SLSP, replacing empirically set fermentation time with a criterion grounded in kinetic, metabolomic and sensory evidence. Fermentation kinetics showed that viable counts peaked at 24 h, remained in stationary phase until 48 h, and then declined. pH stabilized by 24 h and TA plateaued by 48 h, while reducing sugars were largely depleted by 48 h; primary fermentation had therefore largely subsided before 72 h, and the period from 48 to 72 h represents the transition stage in which the system approached a stable state. Within this transition stage, the volatile-flavor profile peaked at 72 h: the total content of VFCs reached its maximum with an ester-dominated profile, all 24 odor-active compounds exhibited $rOAV \geq 1$ at 72 h, and the lipid-oxidation precursor cluster peaked while the background pools of amino acids, fatty acids, and phosphorylated sugars were nearly exhausted. Notably, C5 short peptides continued to accumulate through F96, indicating that prolonged fermentation enriched non-volatile umami taste-active compounds without further improving the volatile aroma.

Correlation analysis was consistent with a proposed metabolic sequence: C1/C3-cluster polyunsaturated fatty acids were depleted over the fermentation course, while C6-cluster hydroxy-fatty acids and jasmonates accumulated in parallel; these lipid-oxidation products showed positive temporal correlations with green/fatty aldehydes and ethyl esters, with both the lipid-precursor layer and the volatile ester layer peaking at 72 h. Beyond 72 h, the content of key odor-active compounds declined: the mushroom-type odorant 1-octen-3-one

fell by approximately 21% from its 72 h level, and 2,4-nonadienal dropped to less than one-third of its 72 h value, while sulfur- and roast-derived volatiles accumulated. Meanwhile, the electronic tongue detected no further significant change in taste attributes between 72 h and 96 h, confirming that prolonging fermentation produced no further improvement in taste attributes. These findings demonstrate that 72 h represents the fermentation endpoint for *Lp. plantarum*-fermented SLSP, at which the accumulation of odor-active metabolites reached its optimum, after logarithmic growth had ceased and the fermentable substrate had been largely depleted. This work provides a transferable analytical framework for endpoint determination in solid-state fermentation of mushroom-derived substrates. The specific 72 h endpoint is substrate- and strain-dependent, but the framework offers a practical basis for the standardized development of fermented S. latifolia products with reproducible flavor quality.

Supplementary Materials: The following supporting information can be downloaded at: https://www.mdpi.com/article/10.3390/fermentation12110533/s1, Table S1: GC×GC-TOFMS data of volatile compounds; Table S2: LC-MS metabolite annotation data.

Author Contributions: Conceptualization and methodology: Z.W. and Z.K.; writing—original draft: Z.W. and Z.K.; investigation: Z.K., J.H., Z.L., L.Z. and X.L.; supervision: Y.L. and D.Z.; visualization: Z.K.; funding acquisition: B.W.; project administration: Z.K., Y.L. and D.Z.; writing—review & editing: Z.W., Z.K. and D.Z. All authors have read and agreed to the published version of the manuscript.

Funding: This work was supported by the Special Project for Public Welfare Research Institutes in Fujian Province (Grant No. 2024R1006003).

Institutional Review Board Statement: Not applicable.

Informed Consent Statement: Not applicable.

Data Availability Statement: The original contributions presented in this study are included in the Supplementary Materials (Table S1 and Table S2), including the 334 annotated metabolites (LC-MS) and 264 volatile flavor compounds (GC×GC-TOFMS). The raw data supporting the conclusions of this article will be made available by the authors on request.

Acknowledgments: The authors thank Fujian Tianyi Edible Fungi Co., Ltd. for providing the SLSP material.

Conflicts of Interest: The authors declare no conflicts of interest.

Abbreviations

The following abbreviations are used in this manuscript: E-nose, electronic nose; GC-IMS, gas chromatography-ion mobility spectrometry; GC×GC-TOFMS, comprehensive two-dimensional gas chromatography-time-of-flight mass spectrometry; LC-MS, liquid chromatography-mass spectrometry; SLSP, *Sparassis latifolia* superfine powder; *Lp. plantarum*, *Lactiplantibacillus plantarum*; *rOAV*, relative odor activity value; VFCs, volatile flavor compounds; PCA, principal component analysis; OPLS-DA, orthogonal partial least squares discriminant analysis; VIP, variable importance in projection; MSI, Metabolomics Standards Initiative; UG, ultrafine grinding; LAB, lactic acid bacteria; TCA, tricarboxylic acid cycle; ADH, alcohol dehydrogenase; LOX, lipoxygenase; CFU, colony-forming unit; VSCs, volatile sulfur compounds; SPME, solid-phase microextraction; RI, retention index.

References

1. Li, Y.; Yang, Y.; Huang, X.; Huang, J.; Dong, C. Molecular and genetic evidence for a tetrapolar mating system in Sparassis latifolia. *Fungal Biol.* **2020**, *124*, 1004–1012. [CrossRef]
2. Zhou, Y.; Chu, M.; Ahmadi, F.; Agar, O.T.; Barrow, C.J.; Dunshea, F.R.; Suleria, H.A. A Comprehensive Review on Phytochemical Profiling in Mushrooms: Occurrence, Biological Activities, Applications and Future Prospective. *Food Rev. Int.* **2023**, *40*, 924–951. [CrossRef]

3. Liu, J.; Zhang, X.; Zhang, J.; Yan, M.; Li, D.; Zhou, S.; Feng, J.; Liu, Y. Research on Extraction, Structure Characterization and Immunostimulatory Activity of Cell Wall Polysaccharides from *Sparassis latifolia*. *Polymers* **2022**, *14*, 549. [CrossRef]
4. Wang, X.; Zhang, X.; Zhang, D. Enhancement of cation exchange and glucose binding capacity, flavonoids release and antioxidant capacity of Tartary buckwheat powder with ultrafine grinding. *Front. Nutr.* **2023**, *10*, 1276017. [CrossRef]
5. Zhang, Y.; Xiao, W.; Han, L. Effects of Multiscale Mechanical Pulverization on the Physicochemical and Functional Properties of Black Tea. *Foods* **2022**, *11*, 2651. [CrossRef]
6. Lu, Q.; Wang, S.; Xue, S.; Yang, D.; Li, L. Comparison of non-volatile flavor compounds in Stropharia rugosoannulata soup processed by different methods. *J. Food Sci. Technol.* **2022**, *59*, 4025–4036. [CrossRef]
7. Venugopal, K.; Satora, P.; Kała, K.; Sułkowska-Ziaja, K.; Szewczyk, A.; Ostachowicz, B.; Muszyńska, B.; Bernaś, E. Fermented, Freeze-Dried Snacks from *Lactarius deliciosus* as a Source of Functional Compounds and Lactic Acid Bacteria. *Molecules* **2025**, *30*, 1566. [CrossRef]
8. Ayar-Sümer, E.N.; Verheust, Y.; Özçelik, B.; Raes, K. Impact of Lactic Acid Bacteria Fermentation Based on Biotransformation of Phenolic Compounds and Antioxidant Capacity of Mushrooms. *Foods* **2024**, *13*, 1616. [CrossRef]
9. Siezen, R.J.; Vlieg, J.E.v.H. Genomic diversity and versatility of Lactobacillus plantarum, a natural metabolic engineer. *Microb. Cell Fact.* **2011**, *10*, S3. [CrossRef]
10. Wang, B.; Zhao, N.; Li, J.; Xu, R.; Wang, T.; Guo, L.; Ma, M.; Fan, M.; Wei, X. Selenium-enriched Lactobacillus plantarum improves the antioxidant activity and flavor properties of fermented Pleurotus eryngii. *Food Chem.* **2021**, *345*, 128770. [CrossRef]
11. Gao, T.; Chen, J.; Xu, J.; Gu, H.; Zhao, P.; Wang, W.; Pan, S.; Tao, Y.; Wang, H.; Yang, J. Screening of a Novel *Lactiplantibacillus plantarum* MMB-05 and *Lacticaseibacillus casei* Fermented Sandwich Seaweed Scraps: Chemical Composition, In Vitro Antioxidant, and Volatile Compounds Analysis by GC-IMS. *Foods* **2022**, *11*, 2875. [CrossRef]
12. Svendsen, C.; Skov, T.; Berg, F.W.J.v.D. Monitoring fermentation processes using in-process measurements of different orders. *J. Chem. Technol. Biotechnol.* **2014**, *90*, 244–254. [CrossRef]
13. Zhao, S.; Zhang, M.; Ran, Y.; Yang, Z.; Dong, R.; He, L.; Jin, W.; El-Aty, A.M.A. Differentiation of volatile organic compounds in chili powders of different spiciness levels via E-nose, HS-GC–IMS, and chemometrics. *Front. Nutr.* **2025**, *12*, 1629925. [CrossRef]
14. Liu, H.; Fu, M.; Wu, J.; Yu, Y.; Si, W.; Xu, Y.; Yang, J. Flavor characterization of aged Citri Reticulatae Pericarpium from core regions: An integrative approach utilizing GC-IMS, GC–MS, E-nose, E-tongue, and chemometrics. *Food Chem.* **2025**, *490*, 144995. [CrossRef]
15. Duan, Y.; Gao, X.; Shi, B.; Yu, M.; Raza, J.; Sun, H.; Wang, Y.; Song, H.; Xu, Y. Characterize the dynamic changes of volatile compounds during the roasting process of Wuyi rock tea (Shuixian) integrating GC-IMS and GC × GC-O-MS combined with machine learning. *Food Chem.* **2025**, *489*, 144931. [CrossRef]
16. Chen, W.; Liu, W.; Liu, Z.; Wang, D.; Lan, X.; Zhan, S.; Feng, X.; Liu, Y.; Ni, L. Insight into the mechanism of roasting-induced characteristic aroma formation in Wuyi rock tea using an "in-leaf" model with isotopic labeling. *Food Chem.* **2025**, *474*, 143174. [CrossRef]
17. Rajendran, S.; Khomenko, I.; Silcock, P.; Betta, E.; Pedrotti, M.; Biasioli, F.; Bremer, P. The Effect of Different Medium Compositions and LAB Strains on Fermentation Volatile Organic Compounds (VOCs) Analysed by Proton Transfer Reaction-Time of Flight-Mass Spectrometry (PTR-ToF-MS). *Fermentation* **2024**, *10*, 317. [CrossRef]
18. Ali, Z.; Mbadinga, U.F.N.; Wen, S.; Hou, X.; Wang, J. Flavor formation through lactic acid bacteria metabolism in traditional Chinese fermented vegetable products. *J. Ethn. Foods* **2025**, *12*, 34. [CrossRef]
19. Hu, Y.; Zhang, L.; Wen, R.; Chen, Q.; Kong, B. Role of lactic acid bacteria in flavor development in traditional Chinese fermented foods: A review. *Crit. Rev. Food Sci. Nutr.* **2020**, *62*, 2741–2755. [CrossRef]
20. Miller, G.L. Use of Dinitrosalicylic Acid Reagent for Determination of Reducing Sugar. *Anal. Chem.* **1959**, *31*, 426–428. [CrossRef]
21. van Gemert, L.J. *Compilations of Odor Threshold Values in Air, Water and Other Media*, 2nd ed.; Oliemans Punter & Partners BV: Utrecht, The Netherlands, 2011.
22. Shen, C.; Cai, Y.; Wu, X.; Gai, S.; Wang, B.; Liu, D. Characterization of selected commercially available grilled lamb shashliks based on flavor profiles using GC-MS, GC × GC-TOF-MS, GC-IMS, E-nose and E-tongue combined with chemometrics. *Food Chem.* **2023**, *423*, 136257. [CrossRef]
23. Hong, K.; Zhang, H.; Han, M.; Nie, X.; Fu, X.; Lei, F.; He, D. A novel four-species microbial consortium for nutritional value improvement of rapeseed meal. *Food Chem.* **2025**, *478*, 143712. [CrossRef]
24. Ma, D.; Li, Y.; Chen, C.; Fan, S.; Zhou, Y.; Deng, F.; Zhao, L. Microbial succession and its correlation with the dynamics of volatile compounds involved in fermented minced peppers. *Front. Nutr.* **2022**, *9*, 1041608. [CrossRef]
25. Hu, X.; Li, D.; Ding, Y.; Zhang, Y.; Ren, C. Characteristic of volatile flavor compounds in 'Fengtangli' plum (Prunus salicina Lindl.) were explored based on GC×GC-TOF MS. *Front. Nutr.* **2025**, *12*, 1536954. [CrossRef]
26. Saud, S.; Xiaojuan, T.; Fahad, S. The consequences of fermentation metabolism on the qualitative qualities and biological activity of fermented fruit and vegetable juices. *Food Chem. X* **2024**, *21*, 101209. [CrossRef]

27. Prasad, R.; Varshney, V.K.; Harsh, N.S.K.; Kumar, M. Antioxidant Capacity and Total Phenolics Content of the Fruiting Bodies and Submerged Cultured Mycelia of Sixteen Higher Basidiomycetes Mushrooms from India. *Int. J. Med. Mushrooms* **2015**, *17*, 933–941. [CrossRef]
28. Goffin, P.; Lorquet, F.; Kleerebezem, M.; Hols, P. Major Role of NAD-Dependent Lactate Dehydrogenases in Aerobic Lactate Utilization in *Lactobacillus plantarum* during Early Stationary Phase. *J. Bacteriol.* **2004**, *186*, 6661–6666. [CrossRef]
29. Xie, A.; Dong, Y.; Liu, Z.; Li, Z.; Shao, J.; Li, M.; Yue, X. A Review of Plant-Based Drinks Addressing Nutrients, Flavor, and Processing Technologies. *Foods* **2023**, *12*, 3952. [CrossRef]
30. Nie, X.; Luo, J.; Chen, H.; Pu, H.; Luo, Q.; Wang, X.; Yu, X.; Liu, D.; Zhao, Z. The potential correlations between cell-free extracts from Rhodobacter sphaeroides grown under low-oxygen conditions and volatile organic compounds in Chinese-style sausage. *Food Chem. X* **2024**, *24*, 101967. [CrossRef]
31. Zhao, L.; Wang, Y.; Wang, D.; He, Z.; Gong, J.; Tan, C. Effects of Different Probiotics on the Volatile Components of Fermented Coffee Were Analyzed Based on Headspace-Gas Chromatography-Ion Mobility Spectrometry. *Foods* **2023**, *12*, 2015. [CrossRef]
32. Su, T.; Chen, Y.; Liu, H.; Gao, Y.; Guo, J.; Li, Y.; Qi, Y.; Qiu, L. The Biosynthesis of 1-octene-3-ol by a Multifunctional Fatty Acid Dioxygenase and Hydroperoxide Lyase in *Agaricus bisporus*. *J. Fungi* **2022**, *8*, 827. [CrossRef]
33. Song, B.; Zhou, Y.; Zhan, R.; Zhu, L.; Chen, H.; Ma, Z.; Chen, X.; Lu, Y. Effects of Different Pesticides on the Brewing of Wine Investigated by GC-MS-Based Metabolomics. *Metabolites* **2022**, *12*, 485. [CrossRef]
34. Wu, Y.; Li, Z.; Zou, S.; Dong, L.; Lin, X.; Chen, Y.; Zhang, S.; Ji, C.; Liang, H. Chemical Composition and Flavor Characteristics of Cider Fermented with *Saccharomyces cerevisiae* and Non-*Saccharomyces cerevisiae*. *Foods* **2023**, *12*, 3565. [CrossRef]
35. Shi, L.; He, W.; Lin, M.; Fu, X.; Li, Y.; Liang, Y.; Zhang, Z. Comprehensive analysis of volatile flavor components in pear fruit spanning the entire development stages. *Food Chem.* **2025**, *485*, 144493. [CrossRef]
36. Sun, J.; Cai, W.; Feng, T.; Chen, D.; Lu, J.; Song, S.; Yao, L.; Sun, M.; Wang, H.; Liu, Q.; et al. Revealing the flavor profile of citrus Pu-erh tea through GC-MS-O and untargeted metabolomics. *Beverage Plant Res.* **2024**, *4*, e009. [CrossRef]
37. Borrajo, P.; Karwowska, M.; Lorenzo, J.M. The Effect of *Salvia hispanica* and *Nigella sativa* Seed on the Volatile Profile and Sensory Parameters Related to Volatile Compounds of Dry Fermented Sausage. *Molecules* **2022**, *27*, 652. [CrossRef]
38. Seriki, A.L.; Alleman, A.B.; Ticak, T.; Baugh, A.C.; Creagh, J.W.; Marx, C.J. Engineered *Methylobacterium extorquens* grows well on methoxylated aromatics due to its formaldehyde metabolism and stress response. *mSphere* **2025**, *10*, e0017125. [CrossRef]
39. Lu, B.; Chen, X.; Ouyang, X.; Li, Z.; Yang, X.; Khan, Z.; Duan, S.; Shen, H. The roles of novel chitooligosaccharide-peanut oligopeptide carbon dots in improving the flavor quality of Chinese cabbage. *Food Chem. X* **2023**, *20*, 100963. [CrossRef]
40. Xuexue, Z.; Xin, H.; Youlan, J.; Chao, W.; Zhonghua, L.; Jianan, H.; Qin, L. Characterization of key aroma compounds and relationship between aroma compounds and sensory attributes in different aroma types of Fu brick tea. *Food Chem. X* **2022**, *13*, 100248. [CrossRef]
41. Li, X.; Zeng, X.; Song, H.; Xi, Y.; Li, Y.; Hui, B.; Li, H.; Li, J. Characterization of the aroma profiles of cold and hot break tomato pastes by GC-O-MS, GC × GC-O-TOF-MS, and GC-IMS. *Food Chem.* **2022**, *405*, 134823. [CrossRef]
42. Steger, M.C.; Rigling, M.; Blumenthal, P.; Segatz, V.; Quintanilla-Belucci, A.; Beisel, J.M.; Rieke-Zapp, J.; Schwarz, S.; Lachenmeier, D.W.; Zhang, Y. Coffee Leaf Tea from El Salvador: On-Site Production Considering Influences of Processing on Chemical Composition. *Foods* **2022**, *11*, 2553. [CrossRef]
43. Zhang, D.; Yang, P.; Liu, K.; Wu, L.; Li, G.; Zhang, H.; Ma, X.; Rong, L.; Li, R. The effective of bacterial community dynamics driven by different starter cultures on the flavor development of Chinese fermented sausages. *Food Chem. X* **2023**, *19*, 100838. [CrossRef]
44. Li, C.; Wang, C.; Deng, J.; Wang, D.; Huang, H.; Zhao, Y.; Chen, S. Inhibition of Biogenic Amines in Fermented Tilapia Surimi by Collaborative Fermentation of *Latilactobacillus sakei* and *Pediococcus acidilactici*. *Foods* **2024**, *13*, 3297. [CrossRef]
45. Liu, G.; Wang, C.; Lu, X.; Qayyum, N.; Xu, X.; Tian, J.; Ma, Y.; Chu, L.; He, F.; Song, Y.; et al. Dynamic variations in the volatile aromatic compound profile of jujube pulp during fermentation by mixed microbial cultures. *Food Chem.* **2025**, *493*, 145743. [CrossRef]
46. Kim, J.; Choi, K.-B.; Park, J.H.; Kim, K.H. Metabolite profile changes and increased antioxidative and antiinflammatory activities of mixed vegetables after fermentation by Lactobacillus plantarum. *PLoS ONE* **2019**, *14*, e0217180. [CrossRef]
47. Mani-López, E.; Mejía-Garibay, B.; Hernández-Figueroa, R.H.; López-Malo, A. Phenyllactic Acid from Lactic Acid Bacteria: A Natural Antimicrobial for Food Biopreservation. *Fermentation* **2026**, *12*, 184. [CrossRef]
48. Chen, Z.; Fang, X.; Wu, W.; Chen, H.; Han, Y.; Yang, H.; Gao, H. Effects of fermentation with Lactiplantibacillus plantarum GDM1.191 on the umami compounds in shiitake mushrooms (Lentinus edodes). *Food Chem.* **2021**, *364*, 130398. [CrossRef]
49. Jabłońska-Ryś, E.; Przygoński, K. Possibilities of Using the New *Lactiplantibacillus plantarum* EK11 Strain as a Starter Culture for the Fermentation of the Fruiting Bodies of Edible Mushrooms. *Foods* **2025**, *14*, 2833. [CrossRef]

50. Cho, S.; Moazzem, S. Recent Applications of Potentiometric Electronic Tongue and Electronic Nose in Sensory Evaluation. *Prev. Nutr. Food Sci.* **2022**, *27*, 354–364. [CrossRef]
51. Bartkiene, E.; Zarovaite, P.; Starkute, V.; Mockus, E.; Zokaityte, E.; Zokaityte, G.; Rocha, J.M.; Ruibys, R.; Klupsaite, D. Changes in Lacto-Fermented *Agaricus bisporus* (White and Brown Varieties) Mushroom Characteristics, including Biogenic Amine and Volatile Compound Formation. *Foods* **2023**, *12*, 2441. [CrossRef]

Disclaimer/Publisher's Note: The statements, opinions and data contained in all publications are solely those of the individual author(s) and contributor(s) and not of MDPI and/or the editor(s). MDPI and/or the editor(s) disclaim responsibility for any injury to people or property resulting from any ideas, methods, instructions or products referred to in the content.